

Observed variation in the decay time of oceanic whitecap foam

Adrian H. Callaghan,^{1,2} Grant B. Deane,¹ M. Dale Stokes,¹ and Brian Ward²

Received 17 April 2012; revised 29 June 2012; accepted 23 July 2012; published 14 September 2012.

[1] Whitecap foam decay times for 552 individual breaking waves determined from digital images of the sea surface are reported. The images had sub-centimeter pixel resolution and were acquired at frame rates between 3 and 6 frames per second at the Martha's Vineyard Coastal Observatory over a 10-day period in 2008, subdivided into 4 observation periods. Whitecap foam decay times for individual events varied between 0.2 s to 10.4 s across the entire data set. A systematic positive correlation between whitecap foam decay time and maximum whitecap foam patch area was found for each observation period. For a given whitecap size within each observation period, the decay times varied between a factor of 2 and 5, with the largest variation occurring during unsteady environmental forcing conditions. Within observation periods, bin-averaged decay times varied by up to a factor of 4 across the range of foam patch areas. Between observation periods, the effective whitecap foam decay time, which we define as the area-weighted mean decay time, varied by a factor of 3.4 between 1.4 s and 4.8 s. We found a weak correlation between decay times and individual event-averaged breaking wave speeds. The variation in the active breaking area across all 4 observation periods was small, indicating relatively uniform surface whitecap area generating potential. We speculate that the variation in the foam decay times may be due to (i) the effect of surfactants on bubble and foam stability, and (ii) differences between bubble plume characteristics caused by a variation in breaking wave type.

Citation: Callaghan, A. H., G. B. Deane, M. D. Stokes, and B. Ward (2012), Observed variation in the decay time of oceanic whitecap foam, *J. Geophys. Res.*, 117, C09015, doi:10.1029/2012JC008147.

1. Introduction

[2] Whitecap coverage can be defined as the instantaneous area of whitecap per unit sea surface area and it is typically expressed as a percentage or fractional value (W). Whitecaps are formed when breaking waves entrain air at the surface forming a submerged bubble plume that appears as a patch of highly reflective foam at the sea surface. In the nomenclature of Monahan and Lu [1990], Stage A whitecaps represent foam generated by actively breaking waves and Stage B whitecaps refer to the decaying whitecap foam patches. Whitecaps are a vivid visual expression of a range of air-sea interaction processes and consequently whitecap coverage measurements have been used to provide estimates of the magnitude of air-sea gas transfer [Woolf, 1997], primary marine aerosol production [de Leeuw et al., 2011], bubble plume formation [Monahan and Lu, 1990] and the whitecap albedo effect [Frouin et al., 1996]. By altering the spectral reflectance of the sea surface, the oceanic brightness

temperature and ocean roughness, estimates of whitecap coverage can help provide necessary corrections to account for whitecap contamination, for the satellite retrieval of earth observation products such as ocean color [Gordon, 1997], sea surface salinity [Camps et al., 2008] and wind vectors [Quilfen et al., 2007]. In fact, the high emissivity signature of whitecaps at microwave frequencies has enabled algorithms to be developed to retrieve W estimates from satellites [e.g., Anguelova and Webster, 2006]. In addition, the statistical distribution of speed and length of actively breaking Stage A whitecaps has been used to estimate momentum flux into the ocean and energy dissipation due to breaking waves [e.g., Phillips, 1985; Melville and Matusov, 2002; Gemmrich et al., 2008; Thomson et al., 2009; Kleiss and Melville, 2010].

[3] Estimates of whitecap coverage can be made by photographing the sea surface and discriminating between whitecaps and unbroken background water. The wind stress acting at the sea surface is the dominant force leading to active whitecap formation and consequently, many empirical relationships relating measured W to wind speed have been presented in the literature (for comprehensive reviews see Anguelova and Webster [2006] and Goddijn-Murphy et al. [2011]). However, when these data sets are compiled there are about 3 orders of magnitude of scatter across nearly all wind speeds indicating that factors other than wind speed need to be included in parameterizations to reconcile results from various studies. Additionally, differences in image collection protocols, image processing methods and image resolution have possibly

¹Scripps Institution of Oceanography, University of California, San Diego, La Jolla, California, USA.

²Ryan Institute, School of Physics, National University of Ireland, Galway, Galway, Ireland.

Corresponding author: A. H. Callaghan, Scripps Institution of Oceanography, University of California, San Diego, 9500 Gilman Dr., La Jolla, CA 92093-0238, USA. (callaghan.adrian@gmail.com)

Published in 2012 by the American Geophysical Union.

contributed to some of this scatter. For example, before the advent of low-cost, sophisticated digital photography considerable effort was required to manually analyze sea photographs to provide the first pioneering wind speed parameterizations of W [e.g., *Monahan, 1971; Toba and Chaen, 1973; Ross and Cardone, 1974; Bondur and Sharkov, 1982*]. However, several published digital image processing algorithms now offer the possibility to automate the analysis of large data sets of digital images that are needed to reduce statistical uncertainty associated with each W data point [e.g., *Mironov and Dulov, 2008; Callaghan and White, 2009; Kleiss and Melville, 2011*]. *Callaghan and White [2009]* and *Callaghan et al. [2008a]* have shown that on the order of hundreds of images taken at minimum time intervals of about 3–4 s are needed to produce estimates of W with an uncertainty of about $\pm 5\%$. In addition, recent whitecap coverage studies have begun to elucidate the roles that wave development, wave-wave interaction, wave-current interaction and wind history, play in influencing the variation of W in addition to wind speed [*Lafon et al., 2007; Sugihara et al., 2007; Callaghan et al., 2008a, 2008b; Goddijn-Murphy et al., 2011*]. When considering 5 recent data sets of W and wind speed measurements, the scatter between data sets is about a factor of 10 [*Lafon et al., 2004, 2007; Sugihara et al., 2007; Callaghan et al., 2008a, 2008b*]. It may be that further improvements in processing algorithms and the adoption of a standard method of analysis could reduce this scatter still further. However, here we explore the idea that at least some of the observed scatter in recent experiments is due to physical causes other than wind speed.

[4] It is generally accepted that at any instant, decaying foam patches or Stage B whitecaps occupy more area than Stage A whitecaps and ratios of Stage B to Stage A whitecap coverage have been estimated at between about 1.5 and 40 [*Bondur and Sharkov, 1982; Monahan and Lu, 1990; Kleiss and Melville, 2010*]. The ratio of Stage B to Stage A whitecap coverage depends on foam persistence; the ratio being larger for more persistent foam. This idea was formalized by *Phillips [1985]* who combined his measurement of wave breaking rate with what Phillips refers to as an average bubble persistence time τ_{bub} to obtain W :

$$W = \int_0^{\infty} \tau_{bub} c \Lambda(c) dc \quad (1)$$

where τ_{bub} is the bubble persistence time, $\Lambda(c)$ is the Phillips parameter (described below) and c is the forward speed of the breaking wave crest. The Phillips parameter is a characterization of breaking wave dynamics in terms of breaking wave speed, and is defined such that $\Lambda(c)dc$ is the meters of breaking crest per square meter of ocean surface observed in the range of speeds $(c, c + dc)$. This parameter can also be defined to account for a directional spread in the horizontal, but we do not consider this here. One of the ideas underlying the Phillips parameter is that the kinematics of breaking waves can be described by knowledge of their speed alone; knowledge of the event scale is not required except insofar as event scale and speed are correlated. Once the Phillips parameter for a given breaking wavefield is estimated, it is impossible to recover information about distribution of the scales of individual whitecaps.

Advances in digital image photography and processing have led to several authors evaluating the Phillips parameter from photographs of the sea surface [*Melville and Matusov, 2002; Gemmrich et al., 2008; Thomson et al., 2009; Kleiss and Melville, 2010*]. These data sets have provided extensive information on the wave breaking rate and total average length of breaking crest.

[5] To date, however, there have been relatively few studies concerning the decay time of oceanic whitecap foam. *Monahan et al. [1982]* measured the decay time of whitecap foam generated by 4 laboratory simulated whitecaps by measuring the area of the decaying foam. *Nolan [1988]* reported on the decay time for 9 events during the HEX-MAX campaign in the North Sea. *Sharkov [2007]* provides similar whitecap foam decay data for 12 breaking wave events in the field from different geographical locations.

[6] Here we present data on the decay time of whitecap foam areas for 552 discrete wave breaking events. In section 2 we describe our study area and image processing methods. In section 3 we show examples of foam decay curves and present the main foam decay data. Section 4 compares our data to previous published work, discusses the implications of our findings for a range of air-sea exchange processes and we speculate on the possible causes for the observed variation in whitecap foam decay times. We present our conclusions in section 5.

2. Study Area and Methods

[7] The present data set was acquired during the Surface Processes and Acoustic Communication Experiment in October and November 2008 (SPACE08) at the Martha's Vineyard Coastal Observatory (MVCO) located south of Martha's Vineyard - see Figure 1 in *Callaghan et al. [2008a]* for the position of MVCO relative to Martha's Vineyard and the bathymetry of the surrounding area. The facilities at the MVCO include the Air-Sea Interaction Tower (ASIT) located 3 km south of Martha's Vineyard in 16 m water depth, an Acoustic Doppler Current Profiler (ADCP) in 12 m of water 1.5 km south of Martha's Vineyard and a meteorological mast located at the MVCO shore station on Martha's Vineyard. Wave data presented here were acquired by the MVCO ADCP and wind speed and direction data from the MVCO shore mast.

2.1. Digital Sea Surface Imagery, Meteorological Data and Oceanographic Data

[8] Digital sea surface images were acquired using a 5 mega pixel Arecont Vision digital CCD camera with a 17.5 mm lens, mounted on the ASIT at a height of 39.2 m above the seabed (approximately 23 m above the mean sea level, depending on the tide) and an angle of 59° from the nadir. The mean image footprint area was approximately 339 m^2 which varied by $\pm 5\%$ depending on the water depth at the ASIT and resulted in a mean pixel resolution of order less than 1 cm^2 . Because of instrumentation limitations, the image sampling frequency varied from between 3 fps to 6 fps. The camera was mounted in a fixed position facing a southeasterly direction toward 150° and roughly 50% of all images acquired were contaminated with sun glint and sky reflection and were not suitable for analysis.

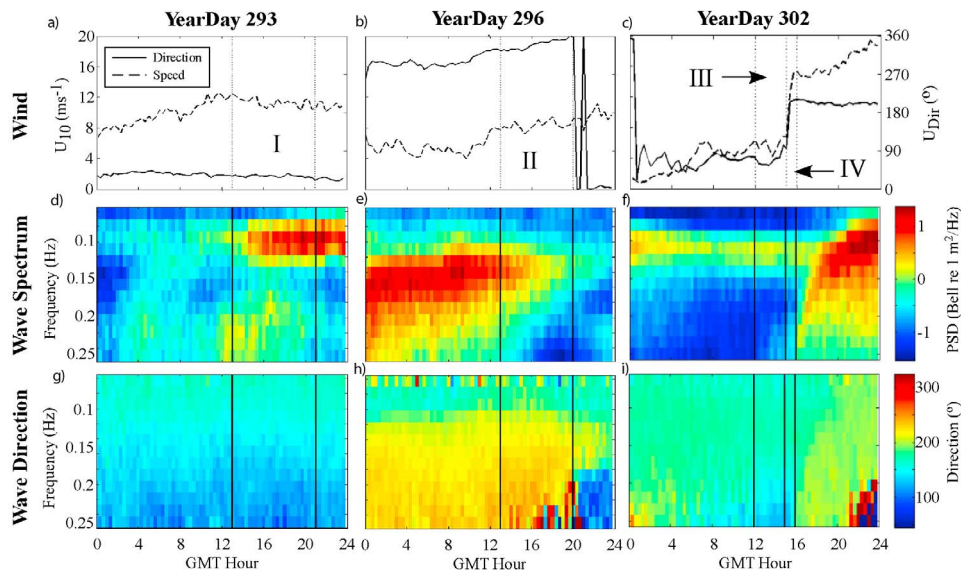


Figure 1. Observations from Year Day (a, d, g) 293, (b, e, h) 296 and (c, f, i) 302. Figures 1a–1c show the wind speed (dashed line) and wind direction (solid line). Figures 1d–1f represent the wave variance frequency spectrum. Figures 1g–1i show the wave directional frequency spectrum. The vertical solid black lines indicate the beginning and end of each observation period. Observational periods I and II were from YD 293 and 296 respectively and observational periods III and IV were from YD 302.

[9] We have chosen three days with images suitable for whitecap foam decay analysis which covered a range of wind speeds from about 5 m/s to 14 m/s. Wind speed and direction data from Year Day (YD) 293, 296 and 302, are shown in Figures 1a–1c (see the map in Figure 1 of Callaghan *et al.* [2008a] for estimates of fetch). Wave variance and directional spectra for these days are shown in Figures 1d–1i. Additionally, representative temporal averages of several wind and wave parameters for each observation period are presented in Table 1.

[10] On YD 293, the observation period is focused on the daylight hours between 1200 GMT and 2100 GMT. During this time the wind direction was steady from the northeast and wind speed decreased slightly but steadily from about 12 m s^{-1} to 11 m s^{-1} over the observation period. The fetch was of order 5 km. A low-frequency peak in the wave spectrum at 0.1 Hz, which is a common feature at the MVCO site, was observed and represents the presence of non-locally generated swell waves propagating from a predominant

southerly direction toward the island of Martha’s Vineyard. The strength of this swell increased in magnitude throughout YD 293. Additionally there was a smaller less energetic peak in the wave spectrum at about 0.225 Hz propagating toward the west. Observation period I represents mixed sea conditions with slowly decreasing wind speed.

[11] On YD 296, wind speed was weaker than on YD 293 but increased from 8 m s^{-1} to 9 m s^{-1} during the observation period between 1200 GMT and 2000 GMT. During this time the wind direction changed slowly but steadily by about 50° from 330° to 20° . The fetch was of order 5 km. In addition to the ever-present northward propagating swell, the wavefield exhibited a decaying sea with a spectral peak at 0.14 Hz which was the result of a strong southwesterly wind event at the beginning of YD 295. This observation period II represents conditions of a decaying wavefield in the presence of slowly increasing wind speed.

[12] The shortest observation period was on YD 302 due to strong contamination of the sea surface images by sun

Table 1. Mean Values for the 4 Observation Periods of Wind Speed (U_{10}) and Direction, Swell Wave Height (H_{swell}), Swell Frequency (F_{swell}), Swell Direction, Wind Wave Height (H_{ww}), Wind Wave Frequency (F_{ww}), Swell-Wave Slope (S_{swell}) and Wind-Wave Slope (S_{ww}) and Wave Direction^a

Observation Period	Wind		Swell Waves				Wind Waves			
	U_{10} (m/s)	Direction (deg)	H_{swell} (m)	F_{swell} (Hz)	Direction (deg)	S_{swell}	H_{ww} (m)	F_{ww} (Hz)	Direction (deg)	S_{ww}
I	11.3	31	0.63	0.1	156	0.018	0.46	0.21	125	0.041
II	8.3	340	0.13	0.09	178	0.003	0.55	0.14	226	0.024
III	5.7	70	0.94	0.11	168	0.030	0.29	0.24	144	0.034
IV	13.7	206	0.89	0.11	169	0.028	0.47	0.24	146	0.055

^aThe slope values were calculated as the product of the relevant wave amplitude and wave number for both the swell waves and wind waves within each observational period.

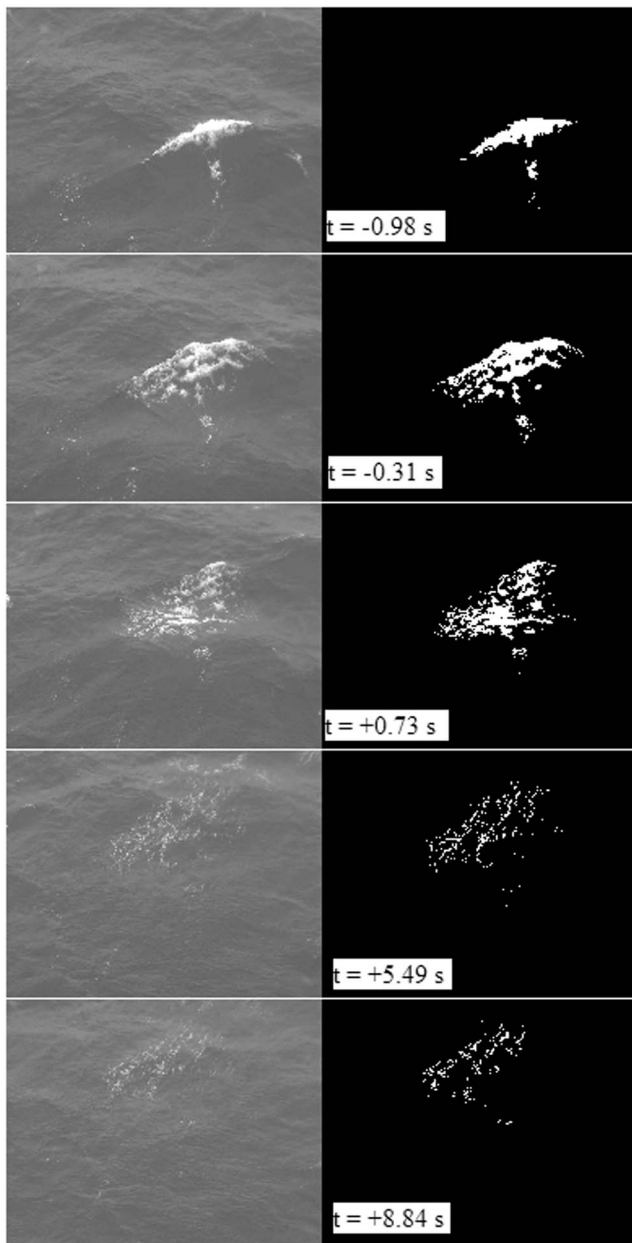


Figure 2. A filmstrip of 5 greyscale and 5 thresholded images depicting whitecap foam from a single whitecap at different times during its evolution. The time is relative to $t = 0$ s which occurs when the measured foam patch area was at its maximum value, A_o . The areas for the whitecap foam are 3.1 m^2 , 6.1 m^2 , 5.6 m^2 , 2.2 m^2 and 1.6 m^2 from top to bottom respectively.

glint after 1600 GMT. Due to an abrupt change in wind speed and direction we divided this period into two. Initially, the wind was weak with speeds between 5 m s^{-1} and 6 m s^{-1} from an easterly direction with a fetch of approximately 20 km. There was a strong peak in the wave spectrum at 0.1 Hz propagating from the south indicating swell dominated conditions (Figures 1f and 1i). The less energetic high

frequency wind waves propagated toward the west. This observation period III is characterized as swell dominated with weak but steady wind. At 1500 GMT there was an abrupt increase in wind speed accompanied by a sharp change in direction from an easterly wind to a southerly wind. As a result the high frequency component of the wave spectrum increased in energy and propagated northward. Observation period IV is characterized as mixed seas with strongly increasing wind speed. The fetch during this period was effectively unlimited, and this is the only observational period for which this is true.

2.2. Image Processing

2.2.1. Image Dimensions

[13] The physical dimensions of each sea surface image were calculated using a combination of known camera height above seabed, water depth, camera inclination angle, calibrated lens focal length and size of the camera CCD chip following *Lippmann and Holman* [1989]. Similarly to *Kleiss and Melville* [2010], the effects of lens distortion were removed from all images using a camera calibration toolbox (J.-Y. Bouquet, Camera calibration toolbox for Matlab, 2006; available at http://www.vision.caltech.edu/bouquetj/calib_doc/). Each pixel was then assigned real world coordinates which allowed the physical dimensions of the whitecaps to be calculated. As a consistency check, the inclination angle of the camera was calculated using the known dimensions of 4 target spherical buoys in the field of view of the camera which supported a floating square instrumented frame. This was found to be equal to 59° , in agreement with the angle measured at the time of camera installation.

2.2.2. Whitecap Foam Identification

[14] To obtain quantitative information on individual whitecaps, the sea surface images were first processed to separate whitecaps from background water following a threshold algorithm described in *Callaghan and White* [2009]. The oblique mounting of the camera on the ASIT introduced a linear gradient in mean illumination between the foreground and background of all images, and this was removed prior to image processing. The image analysis procedure identified supra-threshold regions associated with individual foam patches. Whitecap foam is spatially patchy by nature and a single breaking event is typically composed of multiple foam patches. Foam patch identification through a breaking event started from the moment of first visible air-entrainment and continued until the foam had fully decayed, partially advected out of the image frame or was replenished by foam from another breaking wave. Foam patches were typically tracked over 4–15 s. All the patches associated with an individual whitecap were identified on an image-by-image basis and tagged for analysis by manually specifying a bounding perimeter. The area of foam computed for each image of a selected breaking event was taken to be the sum of the areas of all foam patches within the bounding perimeter. Computing the total foam area in successive images provided a time series of the evolution of the total foam patch area. Figure 2 shows a time series of images from a single breaking wave event to illustrate the result of the processing technique. The manual process of identifying and tracking the foam patches resulted in high fidelity measurements of evolving whitecap

foam patches and ensured no contamination between foam patches.

[15] In addition to foam area, the foam patch analysis was used to determine the active breaking speed, c_{meas} , direction, θ , the breaking crest length, L and the total breaking distance, D . The measurement of c_{meas} is described in section 2.2.3. The image processing was carried out with the Matlab software package and all foam patches were identified as objects by the image processing toolbox. The whitecap foam was typically confined to a single large object during the breaking phase. Occasionally, the breaking crest was returned as two or more individual objects by the choice of threshold due to variations in the along crest breaking pattern. Since the foam tracking procedure was a manual process, these objects were merged if they formed part of the same breaking crest and treated as a single object. Pre-defined Matlab image processing algorithms returned measurements of the breaking wave center of mass, the breaking crest length L and the breaking direction. The total breaking distance D was calculated following

$$D = \sum_{i=1}^{N-1} c_{meas,i} \Delta t \quad (2)$$

where N is the total number of images in the breaking event and Δt is the time interval between successive images.

2.2.3. Measurement of Breaking Wave Speed

[16] The speed of a breaking crest was measured by analyzing pairs of contiguous images during the active breaking phase of an event. The underlying concept is to estimate the forward progression of the breaking crest and to divide by the time interval between images. A problem arises, however, in determining which part of the object identified as a foam patch corresponds to the breaking crest. When objects in successive images overlap, the simplest way to determine the leading edge of the breaking crest is to process a difference image, which is the subtraction of the earlier from the later image. The major axis of the difference image provides an average orientation for the breaking crest, which is used to create a tangent line to the breaking crest. A second tangent line with the same orientation as the first but displaced backward to the leading edge of the crest in the earlier image is calculated. The normal (perpendicular) distance between these tangent lines is then determined and divided by the time difference between the two images to obtain c_{meas} .

[17] A different processing method is required when the objects of successive images do not overlap, which occurs with combinations of high breaking speed and low frame rate. In this case, tangent lines with the same orientation, calculated as the mean orientation of both objects, are computed for each image object. The tangent lines were checked through manual, visual inspection to ensure that they occurred on the true leading edge of the breaking crest in both images. As for the differential image processing, the speed is calculated as the normal distance between the tangent lines divided by the time interval between the frames.

[18] The analysis for c_{meas} yields a speed that is the sum of the true breaking speed, c_{true} , any advection due to the component of surface current in the direction of wave propagation, U_{adv} , and the component of the wave orbital motion of the underlying dominant waves in the direction of

wave propagation, U_{orb} . The estimation of c_{true} from c_{meas} , U_{adv} and U_{orb} is discussed in section 2.2.4. Applying either the two-image or differential-image analysis to a sequence of N images produced $N-1$ estimates of breaking crest direction and speed, where N was a function of breaking duration and the frame rate of the camera. After correcting for advection and wave orbital straining (described in section 2.2.4), the breaking speed time series was used to compute a mean breaking crest speed:

$$\bar{c} = \frac{1}{N-1} \sum_{j=1}^{N-1} c_j, \quad (3)$$

where c_j is the j th speed estimate for an event.

[19] Various authors have employed different image processing methods to measure the speed of a breaking wave from sea surface images and for comparison we provide a very brief overview of these methods. *Gemmrich et al.* [2008] created a differential image and the measured breaking speed was calculated as the distance traveled by the centroid of the differential object between successive images divided by the image sampling time interval. *Gemmrich et al.* assigned a single speed to each breaking event defined as the average of the highest one third measured speeds over the breaking duration, $c_{1/3}$. *Melville and Matusov* [2002] employed a different approach and treated each breaking crest as a collection of small breaking events. They acquired images at 5 Hz and using techniques based on particle image velocimetry, the pixels along the perimeter of a breaking crest were each assigned a breaking speed and direction and this resulted in a broad distribution of breaking speeds for each breaking wave. *Kleiss and Melville* [2010, 2011] employed several methods similar to the approaches of both *Gemmrich et al.* [2008] and *Melville and Matusov* [2002]. Other approaches include a Fourier based technique developed by *Thomson and Jessup* [2009] and an approach using high resolution radar backscatter employed by *Phillips et al.* [2001]. Currently, there is no universally accepted and standardized method for wave speed calculation and we refer readers to these papers for a full description of the various methods.

2.2.4. Advection Correction to Measured Breaking Wave Speed, c_{meas}

[20] The speed of advance of whitecap foam during wave breaking is a combination of the phase velocity of the breaking wave itself and advection due to surface currents and the underlying long wave orbital velocities [*Phillips et al.*, 2001; *Gemmrich et al.*, 2008; *Kleiss and Melville*, 2011]. In addition, it has been shown from laboratory experiments on breaking waves that the measured speed of advance of the whitecap crest (c_{meas}) is some fraction of the computed linear phase speed of the underlying breaking wave (c_{lin}) such that $c_{meas} = \alpha c_{lin}$ where α has been reported to be in the range of 0.7–0.9 [*Rapp and Melville*, 1990; *Banner and Peirson*, 2007; *Kleiss and Melville*, 2011]. The true breaking speed (c_{true}) must be calculated from the measured breaking speed and surface drift, U_{adv} . Following *Kleiss and Melville* [2011]:

$$c_{true} = \frac{\left(\frac{c_{meas}}{\alpha}\right) - \left(\frac{U_{orb}^2 C}{ga} + U_{adv}\right)}{\left(1 - \frac{U_{orb}^2}{ga}\right)} \quad (4)$$

where g is acceleration due to gravity, a is the long wave amplitude, C is the phase speed of the straining long wave, U_{adv} is the speed of advection due to the component of surface current in the direction of wave propagation and U_{orb} is the component of the wave orbital motion of the underlying dominant waves in the direction of wave propagation. The direction of mean water flow is available from the ADCP records and U_{orb} is calculated as described below. We have used $\alpha = 0.9$ following *Kleiss and Melville* [2011].

[21] Calculation of U_{orb} is based on linear wave theory [*Holthuijsen*, 2007] following:

$$U_{orb} = (2\pi f_s a) \left(\frac{\cosh(k_s(d_{ASIT} + a_s))}{\sinh(k_s d_{ASIT})} \right), \quad (5)$$

where f_s , k_s and a_s are the frequency, wave number and amplitude respectively of the dominant component of swell at the ASIT and d_{ASIT} is the water depth at the ASIT. These four parameters were determined as constants for each 20 min interval within each observational period I-IV as follows. An estimate of the single-sided, gravity wave spectral density, $S(f)$, is provided by the ADCP measurements, located 1.5 km to the north of ASIT. Separation of this spectrum into swell and wind-driven components was made possible by noting that the swell always propagated from the south, whereas the direction of the wind-driven waves varied according to the wind direction. Analysis of the wave directional spectrum allowed the determination of a transitional frequency, f_2 , that separated wind and swell components. Given f_2 , f_s was determined by finding the frequency of the peak of $S(f)$ within the swell band: $f_1 \leq f_s \leq f_2$, where $f_1 = 0.0625$ Hz. The swell wave number was determined from f_s and the water depth at ASIT, d_{ASIT} , by solving the gravity wave dispersion relation:

$$4\pi^2 f_s^2 = g k_s \tanh(k_s d_{ASIT}). \quad (6)$$

The amplitude of the swell at the ADCP, a_{ADCP} , was calculated by integrating the wave spectrum between f_1 and f_2 :

$$a_{ADCP} = 2 \sqrt{\int_{f_1}^{f_2} S(f) df}. \quad (7)$$

To account for changing bathymetry (the ADCP was in water 4 m shallower than the ASIT), a_s was determined from a_{ADCP} by assuming conservation of energy [*Holthuijsen*, 2007]:

$$a_s = a_{ADCP} \left(\sqrt{\frac{c_{g,ADCP}}{c_{g,s}}} \right), \quad (8)$$

where $c_{g,ADCP}$ and $c_{g,s}$ respectively are the group velocities of the peak swell component at the ADCP and ASIT. We did not account for any directional changes in the swell waves that may have occurred due to refraction and used the measured wave direction from the ADCP. Additionally this analysis is based upon the assumption that all breaking waves occurred upon the crests of long waves. However, *Phillips et al.* [2001] found that breaking can occur within 60° of the long wave crest. Therefore our

correction may be overestimated by as much as 50%. As a result of the breaking wave speed corrections, the final c_{true} differed from c_{meas} by between -8% to $+16\%$ on average across all observational periods. In further discussions c implicitly refers to c_{true} .

3. Results

[22] In total, our foam decay data are derived from the analysis of 552 individual breaking wave events; 203 from period I, 218 from period II, 91 from period III and 40 from period IV. The analysis of each event produced a temporal record of the evolution of the area of foam produced by the breaking wave from the point of initial breaking to a certain time thereafter when the associated decaying patch of foam could no longer be easily identified or the foam patch was replenished by another breaking wave.

3.1. Observed Characteristics of Whitecap Foam Decay

[23] A whitecap is formed when air is entrained into the water column by the overturning crest of a breaking wave and the evolution of the whitecap can be divided into 3 overlapping phases: the air injection phase, the plume degassing phase and the foam decay phase. During the air injection phase, bubbles are formed and fragmented inside the breaking wave crest. This initial entrainment is termed the acoustically active phase because the formation of bubbles is accompanied by a burst of noise and lasts for a second or so [*Deane and Stokes*, 2002]. Immediately after air entrainment, the whitecap enters the plume degassing phase. During this phase several processes are important to the evolution time-scale of the buoyant bubble plume within the whitecap including turbulent diffusion, advection, dissolution and degassing as the bubbles rise to the surface [*Deane and Stokes*, 2002]. The timescale associated with this phase of whitecap evolution depends strongly on the size of the submerged bubbles and the depth of the bubble plume penetration but may last on the order of several seconds. During the foam decay phase of the whitecap, when the risen bubbles have formed whitecap foam at the air-sea interface, the lifetimes of individual foam cells are controlled by the physics of thin liquid films, cell coalescence and environmental conditions such as surface turbulence, evaporation and direct wind-forcing which may cause the foam cells to rupture. Together, these factors combine to determine the lifetime of the whitecap foam, from genesis to the final stages of decay.

[24] Temporal patterns of foam evolution show an initial rapid growth during the air injection phase followed by a more gradual decay. We are not concerned with the foam growth phase here and similarly to *Monahan and Zietlow* [1969], have chosen to model the decay of whitecap foam with a simple exponential model of the form

$$A(t) = A_o \exp(-t/\tau), \quad (9)$$

where $A(t)$ is the time evolving area of whitecap foam during the decay phase, t is time where $t = 0$ occurs at the time when the foam patch area is at its maximum value, A_o , and τ is a constant we are calling the whitecap foam decay time. Figures 3a and 3b show the time evolution of the area of two individual whitecaps. These events are taken from YD 293 and YD 296 with exponential decay constants of 5.6 s (5.4 s,

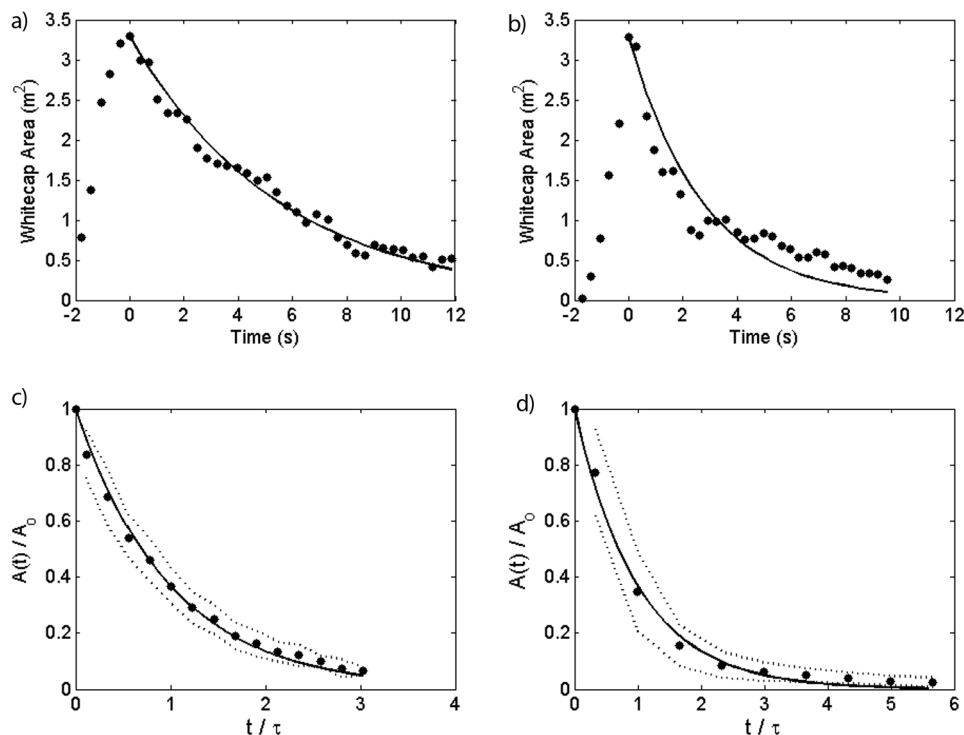


Figure 3. (a, b) Time series' for the area evolution of 2 individual whitecaps (black dots). Time $t = 0$ s is the time of maximum foam patch area, the solid black lines are fitted exponential decay curves with decay times of 5.6 s and 2.7 s respectively. (c, d) Ensemble averaged decay curves from 35 and 42 whitecaps with decay times in the range 4–5 s and 0.5–1 s respectively. The solid lines show the fitted exponential decay curves with decay times of 4.46 s and 0.75 s respectively and the x-axes have been normalized to these decay times. Dotted lines represent 95% confidence intervals.

5.8 s) and 2.7 s (2.4 s, 3.0 s) respectively. Values in parentheses are 95% confidence intervals and R-squared values for each curve were 0.98 and 0.87 respectively. These events have been chosen to show the range of decay curves measured. The whitecap foam data in Figure 3a closely follow an exponential decay while the data in Figure 3b initially decay more quickly than the exponential model which is then followed by a slower decay. Periodic variations in the foam area can be seen toward the end of the decay curve in Figure 3b. Variations like these are typically observed in the later stages of foam decay and are due to the passage of waves, which both compress and stretch the residual foam patch and change the camera perspective by tilting the ocean surface. Since the foam patch is made up of a collection of individual foam cells, its compression in the trough and straining on the crest of a passing wave causes a change in foam cell structure, modifying the area of the foam patch. When calculating the area of each individual pixel we have assumed a flat sea surface and the passing of a wave will result in small deviations in the measured foam patch area due to deviations from a flat surface.

[25] Figure 3c shows an ensemble average of 35 events from YD 293 which have values of τ in the range of 4–5 s. Each individual decay curve was normalized by its maximum area before averaging. The fitted exponential model has a value of τ equal to 4.46 s (4.25, 4.70) with an R-

squared value of 0.99. Figure 3d shows an ensemble average of 42 normalized events with values of τ between 0.5 and 1 s taken from YD 302. The fitted exponential model has a value of τ of 0.75 s (0.68 s, 0.84 s) with an R-squared value of 0.99. While there is some departure from a perfect exponential decay, such deviations are typically on the order of only a few percent of the maximum whitecap area.

[26] The decay phase of whitecap foam is driven by complex physical processes such as fluid drainage from films of individual foam cells, cell coalescence and disjoining pressure effects preceding cell rupture [e.g., *Prud'homme and Khan*, 1995]. In this paper, it is not our goal to explicitly account for each of these physical processes but rather to provide a straightforward way to characterize the decay time of whitecap foam. For this reason, an exponential model of foam decay best suits our needs.

3.2. Distribution of Whitecap Foam Decay Time, τ and Maximum Whitecap Foam Patch Area, A_0

[27] The distribution of τ values for each of the four observation periods is presented in Figures 4a–4d and its smoothed probability distribution function in Figure 5. The number of observations in each of the 4 periods reflects the length of time over which observations were made (9 h, 8 h, 3 h and 1 h for periods I–IV respectively). There is a large variation in values of τ across the 4 observation periods with

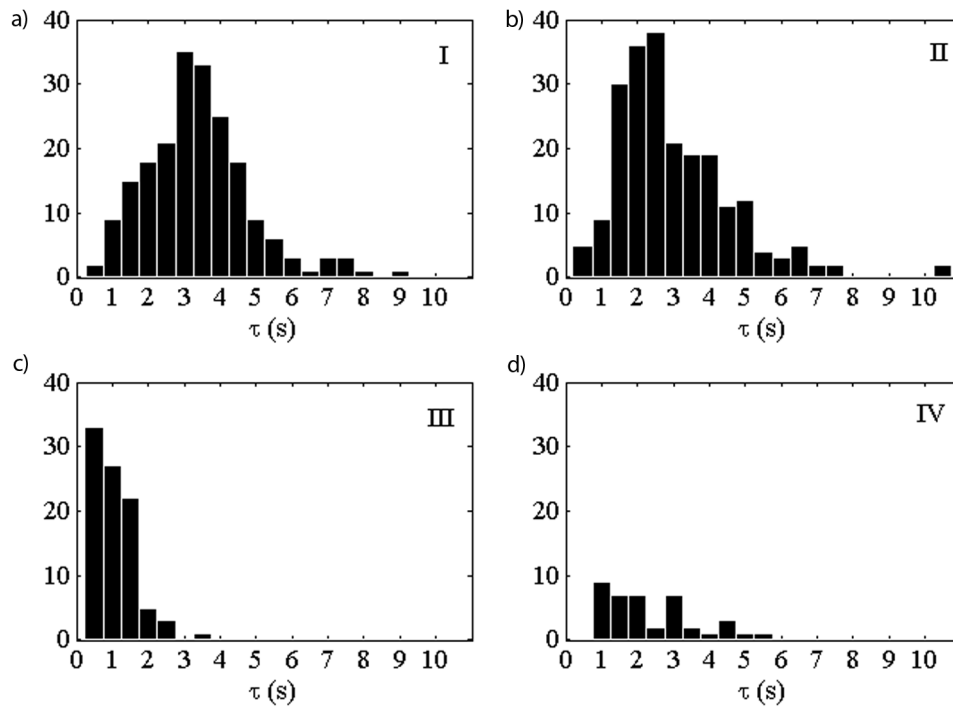


Figure 4. The histograms of the whitecap foam decay times, τ , for each observation period.

minimum and maximum τ values for individual events of 0.2 s and 10.4 s respectively. Period I and period II display a wide range of τ values that lie between approximately 0.5 s and 10.4 s with the majority of whitecaps having foam decay constants in the range of 2–5 s. However, the peak in the distributions for period I and II occurs between 3–4 s and 2–3 s respectively. The τ values for period III show a much narrower distribution with a maximum τ value of approximately 3.5 s. The majority of values lie below 1.5 s and the peak in the distribution lies in the 0.5 s bin. Similarly to period I and II, period IV exhibits a relatively broad range of τ values and its maximum value extends up to 6 s. There is no well-defined peak in this distribution and most of the τ values fall within the range of 1 s to 3.5 s. The absence of a peak in period IV may be a consequence of the relatively small number of observations during this period or the unsteady environmental conditions, but nevertheless there was a substantial increase in the range of τ values which almost doubled from period III. A student's t-test revealed that the sample means for each of the 4 observation periods are statistically different at the 95% confidence level, indicating that the differences in observed mean decay times were not simply a result of sampling statistics.

[28] Figures 6a–6d and Figure 7 display the distribution of A_o values and the smoothed probability density function for each time period respectively. The maximum area of individual foam patches that we resolved in this study was about 26 m² and the majority of foam patches had maximum values that were below 10 m². These observations differ from the results of *Bondur and Sharkov* [1982], who found a peak in the distribution of areas of individual whitecaps in the range 8–16 m² (see their Figure 3, bottom panels). The difference may be due to the difference in image footprint - Bondur and Sharkov made their observations by plane, approximately

100 m above the sea surface with an image footprint of 10,000 m², enabling them to resolve the largest breaking scales. The outer scale of our data set was limited by the image footprint area (approximately 339 m²) because many of the largest breaking waves did not complete the breaking process within the image footprint, and when they did, the surface foam patch was quickly advected out of the field of view. Therefore we were unable to resolve the evolution of the largest whitecaps during the observation periods. Period I has the largest number of A_o values above 6 m² which

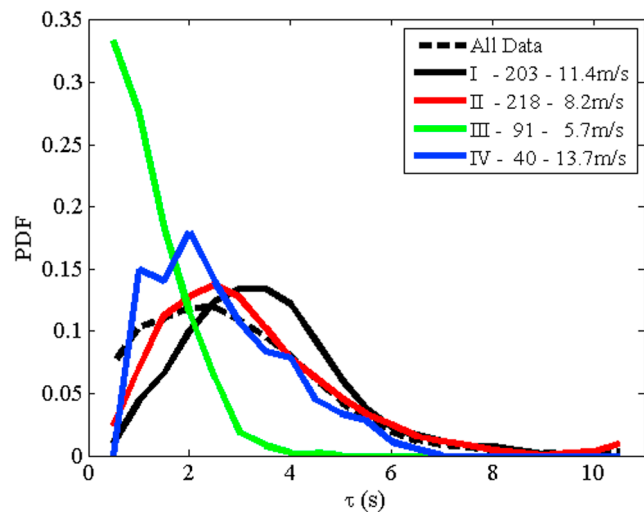


Figure 5. Probability density function of the whitecap foam decay times for the entire data set and for each period. The legend also contains the number of events analyzed and the average wind speed for each period.

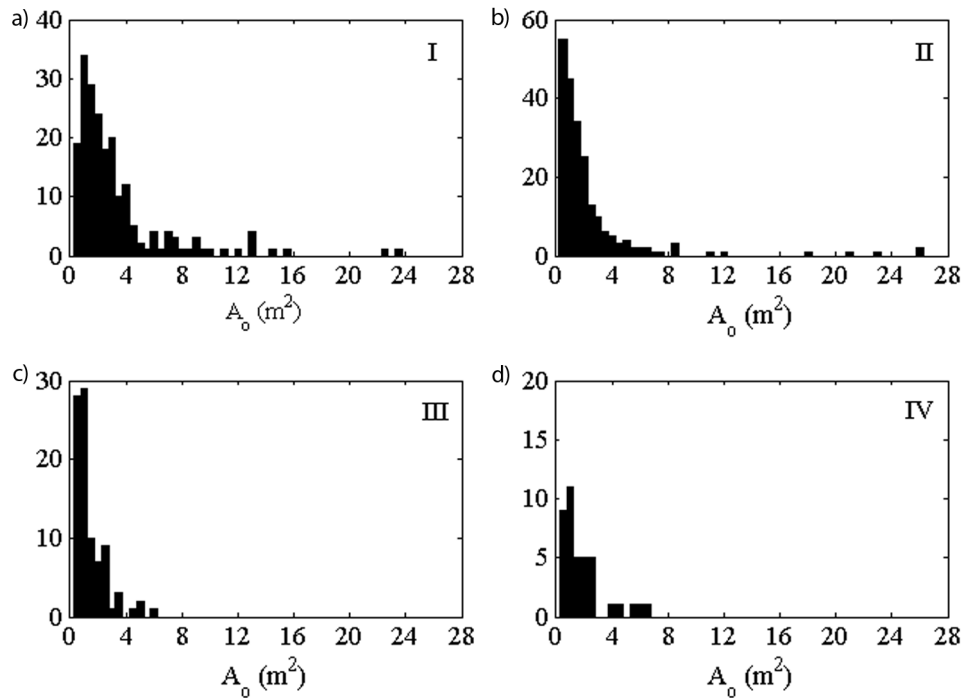


Figure 6. The histograms of the maximum whitecap foam patch area, A_o , for each observational period.

probably reflects the relative strength of the wind during this time period. The peak in the distribution of A_o values in periods II and III lies below 1 m^2 and their distributions have similar shapes but there is a wider range of A_o values in period II than in period III. Period I and period II had the largest steady wind speeds and display a similar range of A_o values which is larger than period III and period IV. A student's t-test revealed that the sample means of A_o for all periods are statistically different at the 95% confidence level except for period IV which is not significantly different from period II and period III at the 95% confidence level.

3.3. Variation of τ With Maximum Whitecap Area, A_o and Mean Breaking Wave Speed, \bar{c}

[29] Along with the foam decay time, τ , and the maximum foam patch area, A_o , other characteristic variables that were measured for each breaking wave event include (i) the mean breaking speed \bar{c} , (ii) the mean breaking crest length, \bar{L} and (iii) the active breaking area, defined as $\psi = D\bar{L}$, where D is the distance over which active breaking takes place (see equation (2)). To determine what the best single descriptor of τ was, we calculated the correlation coefficient, r , between τ , A_o , \bar{c} , \bar{L} and ψ within each observational period following

$$r = \frac{\text{cov}(x, y)}{\sqrt{\text{cov}(x, x)\text{cov}(y, y)}} \quad (10)$$

where $\text{cov}(x, y)$ represents the covariance of variables x and y which is determined by

$$\text{cov}(x, y) = \frac{\sum_i^{N_E} (x_i - \bar{x})(y_i - \bar{y})}{N_E - 1} \quad (11)$$

where N_E is the number of events in the selected period. The correlation coefficients for each observation period are presented in Tables 2a–2d. For all 4 periods, τ was strongly correlated with A_o .

[30] The correlation between τ and A_o can be clearly seen in a scatterplot of the data shown in Figure 8a. Figure 8b shows the same data, but binned and the bin widths were chosen such that the number of points in each bin was constant within each period, but not between periods. The 95% level confidence intervals for estimated population mean for τ are plotted as vertical lines, one per period. Only one representative confidence interval is shown for each

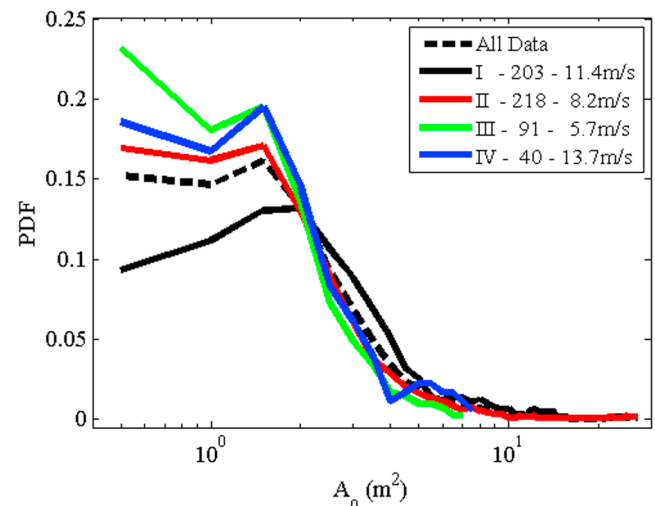


Figure 7. Probability density function of the maximum whitecap foam areas for the entire data set and for each period. The legend is as in Figure 5.

Table 2a. Correlation Coefficients for Observation Period I^a

	τ	A_o	\bar{L}	\bar{c}	ψ
τ		0.65	0.49	0.15	0.54
A_o	0.65		0.75	0.27	0.86
\bar{L}	0.49	0.75		0.28	0.80
\bar{c}	0.15	0.27	0.28		0.48
ψ	0.54	0.86	0.80	0.48	

^aSee text for explanation of symbols.

period since it showed little variability with A_o within a given observation period. The relationship between τ and A_o is well described by a power law for each of the 4 observation periods (see Table 3 for values of power law coefficients). We believe that these data demonstrate a clear and systematic variation in whitecap foam decay time with size of the initial whitecap foam patch on a wave to wave basis. In addition to a systematic variation with A_o , the data in observation period III show significantly reduced values of foam decay from the other three periods.

[31] Figures 9a–9d presents the variation of τ with average breaking wave speed and categorized by value of A_o . No clear dependence between τ and \bar{c} is observed. This is confirmed by inspection of the correlation coefficients in Tables 2a–2d, which all lie below a value of 0.21 except for period III when the correlation coefficient rises to 0.39. For a given range of A_o values, there is a lack of any clear dependence between τ and \bar{c} . The weak correlation between τ and \bar{c} is more likely determined by the distribution of A_o across breaking speeds. The data suggest that the decay time of whitecap foam may be independent of the speed of the breaking wave that formed the initial whitecap.

3.4. Variation of A_o With Active Breaking Area, ψ

[32] Given that τ correlates most strongly with A_o , we wanted to find the best descriptor of A_o in terms of other measured variables. There is a strong positive correlation across all observation periods between A_o and the active breaking area, ψ (see Figure 10a), which is the product of the breaking distance and the breaking crest length. The difference between A_o and ψ is a function of the foam patchiness, with A_o always less than ψ . Regression of the active breaking area with the maximum foam patch area indicates a quasi-linear relationship for the combined data set and for all 4 individual observation periods. The regression coefficients for the combined data set and for the 4 individual observation periods are given in Table 4. For each of the observation periods there is a maximum spread in predicted values of A_o of about a factor of 2 for a given value of ψ . However, plotting the regression relationships on Figure 10b with their 95% confidence intervals reveals that they are not significantly different statistically. The fact that the relationship

Table 2b. Correlation Coefficients for Observation Period II^a

	τ	A_o	\bar{L}	\bar{c}	ψ
τ		0.73	0.52	0.20	0.69
A_o	0.73		0.72	0.24	0.94
\bar{L}	0.52	0.72		0.19	0.76
\bar{c}	0.20	0.24	0.19		0.30
ψ	0.69	0.94	0.76	0.30	

^aSee text for explanation of symbols.**Table 2c.** Correlation Coefficients for Observation Period III^a

	τ	A_o	\bar{L}	\bar{c}	ψ
τ		0.74	0.49	0.39	0.68
A_o	0.74		0.78	0.36	0.90
\bar{L}	0.49	0.78		0.32	0.80
\bar{c}	0.39	0.36	0.32		0.44
ψ	0.68	0.90	0.80	0.44	

^aSee text for explanation of symbols.

between the active breaking area, ψ , and the maximum foam patch area, A_o , is independent of the observation period suggests that the surface whitecap area generating potential of the waves was similar during the 4 observation periods. In other words, if the observed differences in whitecap foam decay time between all 4 periods were due to variations in wave breaking kinematics, this was not detected by our optical measurement technique.

4. Discussion

4.1. Relationship to Prior Work

[33] The variation in decay time of whitecap foam has been reported before, most notably by E. Monahan and coworkers [e.g., *Monahan and Zietlow*, 1969; *Monahan et al.*, 1982; *Nolan*, 1988] and by E. Sharkov and coworkers [see *Sharkov*, 2007, and references therein]. *Monahan et al.* [1982] reported that an ensemble average of 4 events produced a piecewise exponential decay. During the first 5 s of the decay period, the whitecap area decayed exponentially with a decay constant of 1.98 s. From 5 s to 14 s this increased to 3.53 s and it is the value of 3.53 s which *Monahan et al.* [1982] report as the representative decay time constant for their laboratory whitecaps. Using a similar experimental setup, *Monahan and Zietlow* [1969] report a single decay curve for artificial saltwater at 28°C which had an exponential decay constant of 3.85 s.

[34] During the 1986 HEXMAX campaign in the North Sea, *Nolan* [1988] obtained data on the decay characteristics of 9 individual oceanic whitecaps at wind speeds between 10 m s⁻¹ to 15 m s⁻¹. The whitecap decay was modeled as $A(t) = A_o \exp(a + bt)$ and the decay time reported as the reciprocal of constant b . The analysis was carried out on the percentage coverage of the whitecap and not the absolute area. For the nine whitecaps measured, *Nolan* [1988] reports and average decay constant of 4.272 s.

[35] For 4 different times and locations, *Sharkov* [2007] and coworkers measured the time evolution of the foam area of 12 whitecaps using photographs of the sea surface taken at a frame rate of between 1 and 5 frames per second. They too found that $A(t)$ decreased exponentially, as equation (9), from a maximum value. The measured exponential decay

Table 2d. Correlation Coefficients for Observation Period IV^a

	τ	A_o	\bar{L}	\bar{c}	ψ
τ		0.71	0.47	-0.09	0.65
A_o	0.71		0.80	0.03	0.92
\bar{L}	0.47	0.80		0.26	0.81
\bar{c}	-0.09	0.03	0.26		0.16
ψ	0.65	0.92	0.81	0.16	

^aSee text for explanation of symbols.

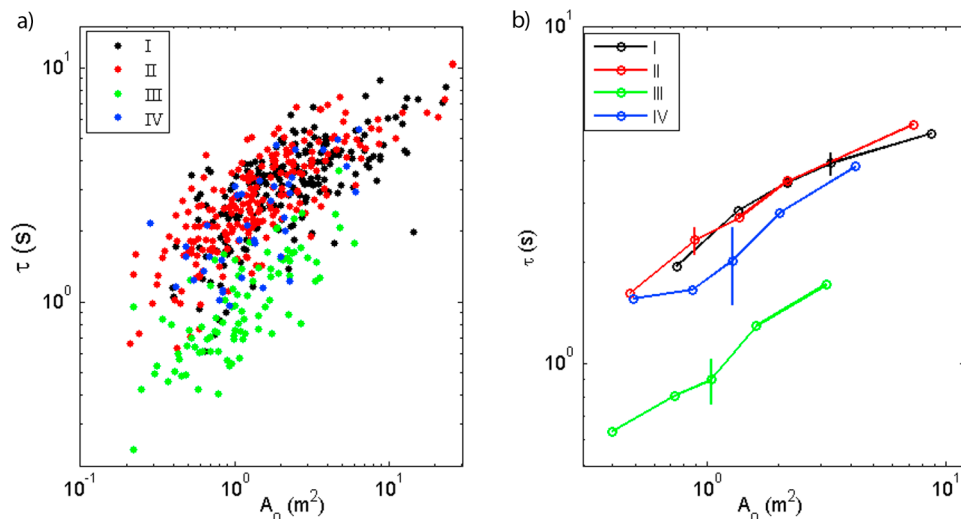


Figure 8. (a) The variation of the whitecap foam decay time with maximum whitecap foam patch area. Black, red, green and blue dots represent periods I, II, III and IV respectively. (b) The data in Figure 8a have been binned for each observation period. The solid vertical lines show representative 95% confidence intervals for each observational period.

times fell within a range from 0.5 s to 7.7 s and the A_o values ranged from 0.3 m^2 to approximately 5 m^2 . No systematic relationship between decay time and A_o was reported and the largest decay time was associated with an event of less than 1 m^2 .

[36] Similarly to these authors, we too find that the mean decay of surface area whitecap foam can be well represented by a simple exponential model. Additionally, the range of exponential decay times presented here largely fall within the range of previously reported values. However, our significantly larger data set shows a systematic variation in τ that is strongly correlated with maximum foam patch size, A_o . In addition there is a statistically significant variation in surface whitecap foam decay with time period. For a given maximum foam patch size, the surface foam decays more quickly during period III than during period I and period II.

[37] To verify that we captured a range of events representative of the in situ environmental conditions for each period, we calculated the Phillips distribution, $\Lambda(c)$. The Phillips distribution is a statistical description of the wave breaking field and can be used to estimate wave energy dissipation, wave to current momentum flux and the number of breaking waves passing a fixed point in space per unit time [Phillips, 1985]. Following Kleiss and Melville [2011] it can be calculated as

$$\Lambda(c) = \frac{1}{A_{tot}\Delta c} \sum_i^{N_E} \left(L_i \left| c - \frac{\Delta c}{2} \leq c_i < c + \frac{\Delta c}{2} \right. \right), \quad (12)$$

where Δc is the breaking speed increment, A_{tot} is the total sea surface area sampled over the time period and L_i is the length of the 'ith' breaking crest whose speed lies within $\pm\Delta c/2$ of c and N_E is the total number of breaking wave events with visible air-entrainment. We did not analyze every breaking event in a given period, rather, breaking events were chosen as being suitable for analysis using criteria described in section 2.2.2. Consequently, we do not have measurements of every value of L_i in each time period and cannot determine the

true A_{tot} with certainty. Additionally, the largest scale events, which could not be tracked within the camera's field of view, are omitted.

[38] Possible approaches to compute an appropriate normalizing factor, A_{tot} , are (i) to integrate the first moment of $\Lambda(c)$ and normalize it such that we obtain breaking rates that are in agreement with previous studies, (ii) to calculate the breaking rate from equation (1) in section 1 using measurements of the whitecap coverage and an estimate of the average bubble persistence time and (iii) to use a multiplicative factor, γ , to account for the fraction of breaking wave crest lengths per unit breaking speed interval that were not measured during each analysis period. The breaking rate is defined as the number of breaking waves passing a fixed point per unit time and can be calculated using the first moment of the Phillips distribution as

$$R = \int c\Lambda(c)dc \quad (13)$$

Field measurements have shown agreement between the first moment of Λ and directly measured breaking rate [Gemrich et al., 2008; Thomson and Jessup, 2009; Kleiss and Melville, 2011]. All three possible normalization approaches mentioned above are subject to uncertain errors. The first approach relies on accurate knowledge of breaking rates for given wind and wavefield conditions,

Table 3. Curve Fitting Results for Variation of τ With A_o ^a

Period	$\tau = k_0 A_o^{k_1}$		r
	k_0	k_1	
I	2.50 (± 0.17)	0.33 (± 0.04)	0.72
II	2.45 (± 0.14)	0.39 (± 0.03)	0.81
III	0.96 (± 0.09)	0.52 (± 0.09)	0.75
IV	1.96 (± 0.33)	0.46 (± 0.14)	0.72

^aCurve fitting was carried out on all the data points and not on the binned data.

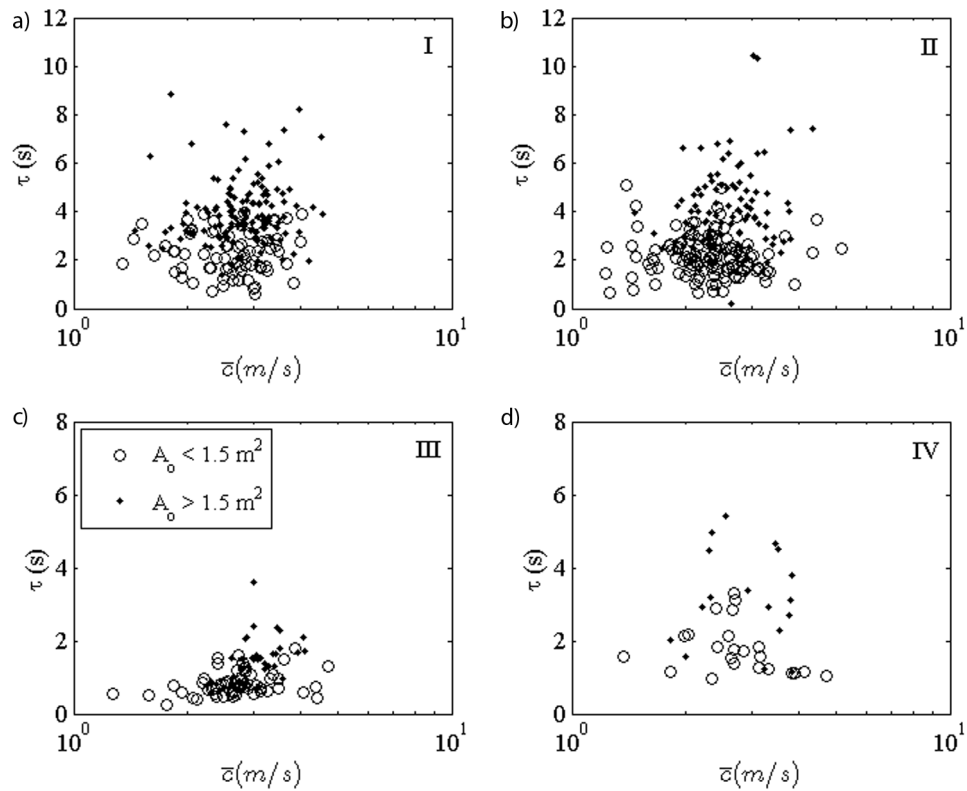


Figure 9. The variation of whitecap foam decay time with the event averaged breaking speed, \bar{c} , for each observational period. The data have been plotted in terms of maximum foam patch area, dots represent $A_o < 1.5 \text{ m}^2$ and circles represent $A_o > 1.5 \text{ m}^2$, where $A_o = 1.5 \text{ m}^2$ is the median value of A_o for the entire data set.

but measured and calculated breaking rates show large variability [Holthuijsen and Herbers, 1986; Gemmrich and Farmer, 1999]. The second approach assumes that total whitecap coverage can be calculated from equation (1), but to the best of our knowledge this has yet to be confirmed with appropriate field data. Additionally, as mentioned in

the introduction above, the scale of individual breaking waves cannot be recovered from the Phillips distribution and the data presented here show that whitecap scale is an important factor determining whitecap foam decay times. For these reasons, and since we want to show the Phillips distribution for qualitative purposes only, we chose to

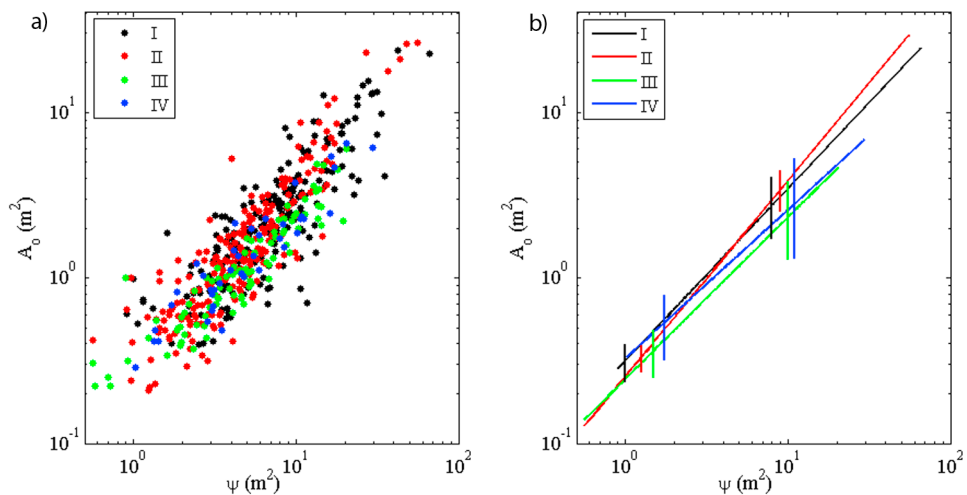


Figure 10. (a) The variation of maximum whitecap foam patch area with the active breaking area. (b) A best fit line for each observational period. The vertical lines show representative 95% confidence intervals for each observational period. The colors are as in Figure 8.

Table 4. Curve Fitting Results for Variation of A_o With ψ^a

Period	$A_0 = k_2 \psi^{k_3}$		r
	k_2	k_3	
All	0.23 (± 0.03)	1.15 (± 0.05)	0.88
I	0.32 (± 0.08)	1.04 (± 0.08)	0.86
II	0.25 (± 0.05)	1.18 (± 0.05)	0.94
III	0.24 (± 0.07)	0.98 (± 0.11)	0.90
IV	0.33 (± 0.11)	0.90 (± 0.13)	0.92

^aCurve fitting was carried out on all the data points and not on the binned data.

follow the third approach outlined above and have used a constant value of $\gamma = 5$ for each observation period. This value is based on our best estimate of the fraction of breaking events that were analyzed during the period. We stress that the uncertainty associated with $\gamma = 5$ is likely to be order $\pm 50\%$ and it also is probably not constant across all observation periods.

[39] The resulting estimates for the Phillips distribution are presented in Figure 11 for each observation period along with other published curves. In general, the shapes and levels of our distributions agree well with previous studies. The maximum values of c measured in each of the 4 time periods falls somewhat short of maximum speeds reported in other studies, which is almost certainly the result of the finite field of view of the camera limiting our analysis to smaller breaking events. The estimated breaking rates for periods I–IV were 32.1 h^{-1} , 25.2 h^{-1} , 26.7 h^{-1} and 31.4 h^{-1} respectively,

which lie within the range of variability reported by other authors [Holthuijsen and Herbers, 1986; Gemmrich and Farmer, 1999]. Given the averaged wind speed values, it is likely that the breaking rate for period III may be an overestimate and we acknowledge that these values are subject to errors. The Phillips parameter analysis demonstrates that the data set includes a representative sample of the breaking wavefield, granted the exclusion of the fastest events.

4.2. Implications of Variable Decay Time of Whitecap Foam

[40] Variability in the decay time of surface foam area has implications for a wide range of air-sea exchange processes, such as primary marine aerosol production flux, energy dissipation estimates from breaking waves, the statistical prediction of total whitecap coverage using the Phillips distribution and parameterizations of whitecap coverage itself.

4.2.1. Primary Marine Aerosol Production

[41] We begin first by exploring the implications of variable foam decay time for modeling the production of primary marine aerosols using the whitecap method. The primary production of marine aerosols is described by the function, $f_{wc}(r)$, which is the size-dependent number of aerosols produced per second per unit whitecap area, where r is the aerosol radius at a specified value of air humidity (80% is often used). The whitecap method combines laboratory measurements of $f_{wc}(r)$ with a canonical whitecap time decay constant and a parameterization for whitecap coverage to calculate the total flux of particles: $f_{tot}(r)$ [Lewis and

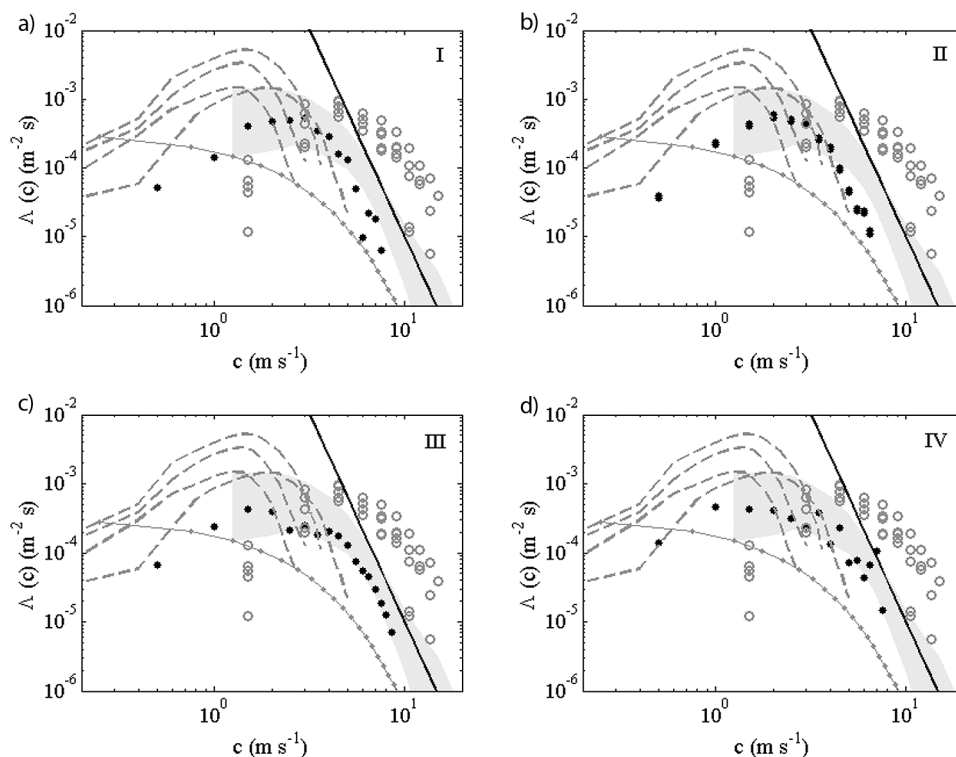


Figure 11. The estimated Phillips $\Lambda(c)$ distribution for each of the 4 periods displayed as solid black dots. Each panel also shows previously published Λ distributions from various authors as follows. Thin gray line with dots from Melville and Matusov [2002], open gray circles from Gemmrich et al. [2008], dashed gray lines from Thomson et al. [2009], gray area from Kleiss and Melville [2011] and the solid black line is representative of the theoretical c^{-6} curve predicted by Phillips [1985].

Table 5. Values of τ_{eff} for the Entire Data Set and for Each Period^a

	All	Period I	Period II	Period III	Period IV
τ_{eff} (s)	4.2	4.4	4.8	1.4	3.1
$\tau_{eff} / 3.53$ s	1.19	1.25	1.36	0.41	0.88

^aAlso shown is the ratio of τ_{eff} to the decay constant of 3.53 s reported in *Monahan et al.* [1982] and widely used in the whitecap method for estimating the size dependent production flux of primary marine aerosols.

Schwartz, 2004]. It is assumed that the total aerosol production flux can be written as:

$$f_{tot}(r) = f_{wc}(r) \times W. \quad (14)$$

Monahan et al. [1982, 1986] pioneered this method and measured the total number of aerosols per radius size per unit volume, $\Delta n(r)$, produced within a controlled experimental volume, V from a whitecap of initial area, $A_{wc,0}$ that decayed with an exponential time constant. The whitecap source function is then given by:

$$f_{wc}(r) = \frac{\Delta n(r)V}{A_{wc,0}\tau}. \quad (15)$$

Equation (15) assumes that all whitecap areas have the same decay time, τ , and that $\Delta n(r)V/A_{wc,0}$ is constant, thereby implying that all whitecaps have the same aerosol producing potential. This assumption allows the total aerosol production flux to be calculated from equation (14) using estimates of f_{wc} and a parameterization for the whitecap coverage.

[42] Our data show variable whitecap foam decay times and therefore the value of τ in equation (15) cannot be assumed to be constant across whitecaps of different scale or between observation periods. We can, however, estimate a single effective decay time, τ_{eff} , that encompasses the combined effect of variable τ on $f_{wc}(r)$ for a range of whitecaps sizes within a given time period. For M whitecaps, the actual total number of particles produced per unit whitecap area per unit second per radius increment is

$$f_{wc}(r) = \frac{\sum_{i=1}^M \Delta n_i(r)V}{\sum_{i=1}^M A_{wc,oi}\tau_i}. \quad (16)$$

An effective decay time can be defined such that:

$$\sum_{i=1}^M A_{wc,oi}\tau_i = \tau_{eff} \sum_{i=1}^M A_{wc,oi}, \quad (17)$$

and τ_{eff} is thus equal to the area-weighted mean of all individual foam decay times:

$$\tau_{eff} = \frac{1}{\sum_{i=1}^M A_{wc,oi}} \cdot \sum_{i=1}^M A_{wc,oi}\tau_i. \quad (18)$$

Equation (18) provides an expression for calculating the effective whitecap decay time, which replaces τ in equation (15).

[43] Often a value of 3.53 s, as determined by *Monahan et al.* [1982], is used in equation (15) [*Lewis and Schwartz*, 2004]. Subsequent to *Monahan et al.* [1982], *Monahan and Lu* [1990] give a range for τ of 3.5–4.3 s. Table 5 shows τ_{eff} calculated for the entire data set and for each individual time period and also the ratio of these values to 3.53 s. Emphasizing the assumption that all whitecaps have the same

aerosol production potential, our data imply that calculations of $f_{wc}(r)$ based on the assumption that τ is constant could be in error by between +36% to –59%.

4.2.2. Whitecap Coverage

[44] As noted earlier, the combined 5 most recent W data sets show about a factor of 10 scatter at all wind speeds, and combined historical parameterizations show significantly more variation - about 3 orders of magnitude. Some of this scatter probably relates to differing sampling and processing approaches. However, there are also environmental factors implicated. For example, wavefield composition and development, wave-current interaction and wind history all affect W . This is not surprising given that breaking rate and the scale of breaking waves change depending on the wavefield development and composition [*Dulov et al.*, 2002; *Gemmrich et al.*, 2008], and both these parameters can be expected to impact W . Therefore the total instantaneous whitecap coverage is a function of breaking rate, breaking scale and foam decay processes.

[45] Of all implicated environmental parameters, foam decay time may be expected to be a primary determinant of W . Images of whitecap foam are comprised of both actively breaking Stage A whitecaps and decaying Stage B whitecaps. However, the literature indicates that Stage B whitecaps always dominate total whitecap coverage [*Monahan and Lu*, 1990; *Bondur and Sharkov*, 1982; *Kleiss and Melville*, 2010] and variation in the persistence of Stage B foam should therefore be an important factor in determining W . While variations in τ across breaking scales within a given observational period can always be averaged out, variations in the mean value of τ across observational periods cannot. For this study, the effective foam decay time varied by up to a factor of 3.4 between the 4 periods, which suggests that some fraction of the observed scatter within and between whitecap coverage data sets could be related to varying foam decay times. Even though some of the scatter in W may be understood in terms of variable foam decay time, it may prove difficult to reconcile the scatter between data sets of total whitecap coverage from diverse geographical locations taken at different times of the year until all the factors affecting the process of whitecap foam decay are understood.

4.2.3. Wave Energy Dissipation

[46] It has been suggested that whitecap coverage should scale with the rate of energy loss due to breaking waves [e.g., *Ross and Cardone*, 1974; *Monahan and O'Muircheartaigh*, 1986; *Zhao and Toba*, 2001; *Hwang and Sletten*, 2008] and several of these authors have presented parameterizations of W in terms of wave energy dissipation, ϵ . By assuming that the wave growth rate is an order of magnitude less than the wind energy input, parameterizations for the rate of wind energy input to the wavefield can be used as an estimate for the amount of energy dissipated by breaking waves. Wave energy dissipation can therefore be estimated from measurements of the wind speed, the dominant wave frequency and the significant wave height [e.g., *Hwang and Sletten*, 2008]. Using a compiled data set of 103 W , wind and wave measurements from previous studies, *Hwang and Sletten* [2008] have demonstrated a strong relationship between W and ϵ , but the data exhibited scatter of about 2–3 orders of magnitude, comparable to the observed scatter between wind speed and W . This approach to parameterizing W is

potentially of great value because it combines wave and wind speed data to provide a multiparameter approach to estimating W that could prove more effective than a wind speed only parameterization. However, since wave energy is dissipated during active breaking only, as represented by Stage A whitecap coverage, W_A , it is currently not known whether measurements of the total whitecap coverage (Stage A + Stage B) should be used as an indicator of energy dissipation. In section 4.4.4, we speculate that causes of variable whitecap foam decay may depend upon influences from surfactants. Additionally, we speculate that the volume of air entrained during wave breaking, which may be used as an indicator of breaking strength, could also be important. However, until all the physical factors affecting the rate of decay of whitecap foam are understood, it may be more prudent to relate wave energy dissipation to Stage A whitecap coverage as opposed to total whitecap coverage.

4.3. Potential Causes of Observed Variations in Whitecap Foam Decay

[47] Bubbles produced by breaking waves provide the source term for whitecap foam observed at the sea surface. Therefore, physical quantities that affect the formation and evolution of sub-surface bubble plumes, along with factors that affect foam stability are likely to cause variations in foam decay times.

4.3.1. Temperature and Salinity

[48] Variations in water salinity and water temperature may both play a role in bubble plume dynamics and subsequent foam evolution. Bubbles in water are stabilized against coalescence by the addition of salt [Pounder, 1986; Henry, 2010]. Monahan and Zietlow [1969] report that laboratory generated salt-water whitecaps persist for 50% longer at the water surface than fresh-water whitecaps of similar dimensions and formation mechanism. Peltzer and Griffin [1988] have demonstrated that increasing salinity from 0 PSU to 16 PSU increases the lifetime of marine foam but this stabilizing effect plateaued and changed insignificantly at higher values of salinity typical of oceanic levels. Changing the temperature of seawater from 0°C to 30°C reduces its kinematic viscosity by about 50%. But, studies trying to elucidate the role of water temperature on whitecap formation and lifetime have provided conflicting results [e.g., Monahan and O'Muircheartaigh, 1986; Wu, 1988]. Monahan and O'Muircheartaigh [1986] suggest for a given input of wave energy to the wavefield, wave breaking rate should increase with decreasing water viscosity at higher water temperatures. Pounder [1986] has suggested that increasing water temperature leads to a decrease in mean bubble size and an increase in bubble density thereby leading to longer bubble risetimes which could sustain decaying foam patches for longer during the degassing phase only. Notwithstanding these effects, variations in salinity (between 31.52 PSU and 31.77 PSU) and temperature (between 13.8°C and 15.9°C) in the SPACE08 experiment were not significant and unlikely to be the cause of the observed variability in foam lifetime.

4.3.2. Soluble and Insoluble Surfactants

[49] Surfactants play a central role in the stability of foams. Surfactants, also known as surface active substances, are organic compounds containing both hydrophilic and hydrophobic chemical groups that preferentially accumulate

at two phase boundaries such as the air-water interface [Manev and Nguyen, 2005; Wurl et al., 2009]. It has been suggested by Phillips [1985], Monahan and Lu [1990] and Sharkov [2007] that surfactants may play an important role in the lifetime of whitecap foam. In the field of thin film physics, it is well known that the presence of surfactants is a necessary condition to stop foam from decaying within a few milliseconds after formation by lowering the surface tension of water [Sheludko, 1967; Weaire and Hutzler, 1999; Manev and Nguyen, 2005; Henry, 2010]. Gradients in the concentration of surfactants adsorbed onto foam cell surfaces give rise to Marangoni forces that act to oppose the gravity driven fluid drainage from within a foam cell wall [Pugh, 1996]. Foam lifetime depends on both the fluid drainage rate when the thin film wall is >100 nm thick and also subsequent intermolecular forces that become important at film thickness of <100 nm. Thin films are prone to rupture at a critical film thickness of circa 50 nm [Manev and Nguyen, 2005; Henry, 2010]. However, the intermolecular forces, which include Van der Waal forces, electrostatic forces and steric effects, can further stabilize the foam cell at the critical thickness or act to destabilize and rupture the foam cell. The intermolecular forces are collectively known as the disjoining pressure and whether they destabilize or stabilize foam cells depends on the surfactant type and concentration [Manev and Nguyen, 2005]. For example, the presence of insoluble surfactants may stabilize marine foams at low concentration but become destabilizing at higher concentration [Garrett, 1967a].

[50] Surfactants are known to be present within the ocean and to accumulate at the air-sea boundary [Garrett, 1967b; Liss, 1975]. They are also known to play a role in air-sea gas exchange and surface capillary damping [e.g., Jähne et al., 1984; Salter et al., 2011]. The primary source of surfactants in the ocean is from the degradation of phytoplankton [Žutić et al., 1981] or zooplankton grazing [Kujawinski et al., 2002]. Surfactants can be present throughout the entire water column and form a sea surface microlayer (SSM) [Williams et al., 1986]. The thickness of the SSM has been reported to be in the range of 1–1000 μm [Liss and Duce, 1997] and it is known to concentrate many surfactant compounds such as carbohydrates, proteins and lipids [Wurl et al., 2011]. The composition of the SSM can be changed by scavenging bubbles that become coated in surfactants as they rise through the bulk water and then burst at the sea surface [Liss, 1975] and also via a process known as competitive adsorption when the SSM is compressed and dilated or simply left to age. Competitive adsorption describes the process whereby more hydrophilic soluble surfactants are desorbed from the SSM into the bulk water below in favor of adsorption of more hydrophobic surfactants [Garrett, 1967b; Bock and Frew, 1993].

[51] Very little systematic work has been done to elucidate how surfactants and the SSM affect open ocean whitecap foam lifetime, but there have been some relevant laboratory experiments. Ternes and Berg [1984] and Garrett [1967a], hereafter referred to as TB84 and G67 respectively, carried out laboratory-based, single bubble experiments to determine the roles of insoluble and soluble surfactants on bubble lifetime in fresh and salt water. Both studies showed that insoluble surfactants that form monomolecular layers increased bubble lifetimes at film pressures of order 1mN m^{-1} but

tended to decrease bubble lifetime at higher film pressures. Film pressures were increased by laterally compressing the surface layer. The film pressure (π) is defined as the difference between the surface tension of pure water (σ_o , 72.75 mN m⁻¹ at 20°C) and that of water with surfactants (σ) written as $\pi = \sigma_o - \sigma$ [Henry, 2010]. Both G67 and TB84 found that for a range of insoluble surfactants, maximum bubble lifetimes in the range 4–30 s occurred at $\pi \approx 1$ –2 mN m⁻¹, but that bubble lifetimes generally decreased at π values greater than 1–2 mN m⁻¹. Bubble lifetimes tended to show an abrupt decrease of between 30%–70% at their critical film pressure, π_{crit} which occurred between about 8–20 mN m⁻¹ across the range of insoluble surfactants [Garrett, 1967a]. The critical film pressure marks the point at which the insoluble surfactant layer changes its molecular packing structure, collapses and fractures and loses its ability to create Marangoni forces [Ternes and Berg, 1984].

[52] G67 extended his study to include two natural seawater samples that contained soluble and insoluble surfactants but had different levels of dissolved organic matter which were reported as organically rich and less-rich. Maximum bubble lifetimes occurred at film pressures of *circa* 1 mN m⁻¹ and lifetimes decreased steadily with increasing film pressures. The maximum bubble lifetimes were 135 s for the organically rich sample and 20 s for the organically less-rich samples, which decreased to about 10 s and 4 s, respectively, at film pressures of 4 mN m⁻¹. G67 suggests that bubbles formed in the seawater samples were initially stabilized by both soluble and insoluble surfactants scavenged as the bubbles rose to the surface. However, at higher film pressures, the bubble lifetimes in both samples approached values similar to those for the insoluble surfactants.

[53] The range of film pressures required to alter bubble lifetime (1–10 mN m⁻¹) are commonly observed in the ocean. For example, Barger *et al.* [1974] found film pressures in the range 1 mN m⁻¹ or less for rippled, apparently clean water and up to 23 mN m⁻¹ within sharply defined, broad band slicks. Film pressure values of 10–16 mN m⁻¹ were typical within these slicks. There were also measurement conditions during low wind speeds when most of the sea surface was slicked and film pressures of 7–8 mN m⁻¹ were observed. More recent *in situ* measurements of slicks have been reported by Ermakov *et al.* [1992]. Film pressures outside slicks were all within 1 mN m⁻¹ of uncontaminated seawater, whereas pressures inside slicks were in the range 4–7 mN m⁻¹.

[54] Through surface convergence or compression, competitive adsorption processes can change the composition of the SSM because soluble surfactants can be desorbed from the SSM into the bulk water below, thereby favoring the presence of insoluble surfactants within the SSM [Garrett, 1967b; Bock and Frew, 1993]. Therefore, under compression, and in the presence of soluble and insoluble surfactants, the SSM could have an increasingly destabilizing effect on bubble lifetime irrespective of the concentration of soluble surfactants within the bulk water as demonstrated by G67. Studies of natural ocean surface films reported by Bock and Frew [1993] have shown that for similar film pressures, different SSM samples can have different ratios of soluble to insoluble surfactants implied from their surface elasticities. In conditions of high productivity the SSM had a higher ratio of soluble to insoluble surfactants than in conditions of low productivity. They note that aging of the SSM allows more

time for competitive adsorption processes to push soluble surfactants out of the SSM and into the bulk water below implying the importance of time history to SSM composition. Similarly to compression, surface divergence or dilation can lead to compositional changes within the SSM. Soluble surfactants are more mobile than insoluble surfactants, thereby allowing them to repair the SSM more rapidly than insoluble surfactants [Garrett, 1967a]. Therefore, under conditions of vigorous wave breaking, frequent SSM disruption may favor a higher soluble to insoluble surfactant ratio. Indeed, G67 noted that at least 30 s to 1 min needed to pass to allow the insoluble surface layer to reform in order to achieve consistent bubble lifetime statistics at discrete film pressures.

[55] The preceding discussion points to a complex relationship between surfactant composition, surfactant transport and the resulting rheological properties of the sea surface. A range of processes (e.g., surface convergence and divergence, bubble scavenging, competitive adsorption, aging) can change the composition of the SSM or the ratio of insoluble to soluble surfactant within the SSM which may have important implications for whitecap foam stability and lifetime.

4.3.3. Bubble Plumes and Breaker Type

[56] Air entrainment beneath breaking waves provides the bubble source term for surface whitecap foam. Within the acoustically active phase of bubble plume evolution, it has been shown that bubble size spectra can exhibit a double power law distribution with slopes that intercept at the Hinze scale [Deane and Stokes, 2002]. Below bubble radii of order 1 mm, the slope of the bubble size distribution is about $-3/2$, whereas above scales of 1 mm, the slope is of order $-10/3$. Given the size dependent rise speed of bubbles with radii up to 0.7 mm, and the greater tendency for small bubbles to dissolve, these slopes exhibit rapid temporal change. In addition to these general features, wind wave laboratory studies of paddle-steepened wind-forced freshwater breaking waves by Leifer and de Leeuw [2006] and Leifer *et al.* [2006] have shown that bubble plumes can exhibit wide heterogeneity in terms of plume lifetime, plume penetration depth, bubble volume and void fraction. In their work, Leifer and coworkers found that plume lifetimes varied by almost a factor of 4, plume penetration depth and void fraction varied by a factor of 10 and plume volume varied by several orders of magnitude. These authors created a bubble plume classification system based upon bubble density, penetration depth and plume horizontal scale. They also showed that interaction between different bubble plumes significantly altered their combined characteristics.

[57] In terms of bubble plume density, Leifer and de Leeuw [2006] noted that “dense bubble plumes were produced at fetches where the wave field was well developed” and these dense plumes were characterized as having larger bubble and plume volumes than diffuse plumes. Consequently, the dense plumes required greater formation energy, they generally had larger penetration depths and persisted longer in comparison with diffuse plumes. Indeed, Leifer *et al.* [2006] showed that the highest proportion of dense plumes occurred in the region of the tank with the largest average breaking wave height. They noted that the probability of dense plume formation increased with increasing wave breaking intensity which coincided with a shift from spilling to plunging breaking waves. Leifer and coworkers did not report any information on the surface area of individual breaking waves so it is

unknown how the surface manifestation of breaking waves as whitecaps changed with breaker type and intensity. It is known that the amount of energy dissipated in breaking waves per unit length is a strong function of breaking wave speed [Duncan, 1981], but recent work also shows a strong dependence on wave slope [Romero *et al.*, 2012]. Laboratory results also generally show that plunging breakers typically result in larger penetration depths than spilling breakers (G. Deane and M. D. Stokes, unpublished experimental data, 2002). For a given breaking wave speed, the energy dissipated is therefore expected to depend on the wave height, wave slope and breaker type.

[58] The measurement of whitecap foam area from sea surface images presented here captures the 2-dimensionality of time-evolving surface foam patches but as currently understood, provides no direct information on the bubble plume penetration depth or the bubble plume density. From the results of Leifer and de Leeuw [2006], Leifer *et al.* [2006] and Romero *et al.* [2012], and given that bubbles produced during active breaking provide the source term for whitecap foam, it is reasonable to assume that variations in foam decay time could reflect variations in the density of bubble plumes from breaking waves which in turn may be dependent on wave breaking strength and breaker type. The likely causal relationship between whitecap persistence and plume dynamics has already been pointed out by Monahan and O’Muircheartaigh [1986], who have contended that the characteristic decay time is a function of “the terminal rise velocity of the small bubble fraction that contributes to the whitecap subsurface bubble cloud,” and that the Stage B whitecap dies out as soon as there is no longer a significant bubble flux to the sea surface.

4.3.4. Speculations on the Effect of Surfactants and Bubble Plume Properties on the Decay Time of Whitecap Foam

[59] From the preceding discussions in section 4.3.2 and 4.3.3, it is clear that relatively minor film pressures play a significant role in changing fluid film stability and bubble plumes characteristics can exhibit a wide range of variability. The results of the studies of Garrett [1967a], Ternes and Berg [1984], Bock and Frew [1993], Leifer and de Leeuw [2006] and Leifer *et al.* [2006] has led us to speculate on the role of surfactants and bubble plume variability on whitecap foam decay times.

[60] The increase in whitecap foam decay time with increasing A_o for all periods may be indicative of several different foam stabilization mechanisms. First, larger whitecaps may lead to deeper penetration depths of bubble clouds during breaking. This could increase the potential for the coating of bubble surfaces with surfactants leading to greater stability when at the sea surface. Second, whitecap foam patches may exhibit a size dependent self-sustaining property. The foam patch decays through foam cell coalescence and rupture. As each foam cell ruptures, it forms film droplets and jet droplets, some of which are transported into the atmosphere as aerosols and the remainder are deposited back onto the sea surface. If we suppose that the fraction of surfactant that is not transported away from the local area via aerosol transport is re-adsorbed onto the underlying foam patch, the remaining foam cells may increase in stability due to increases in surfactant concentration. Larger areas of foam could therefore have a larger potential for re-adsorption of

surfactant. Lastly, our measurement of foam decay only relates information about the decay of the surface area of foam patches and provides no information on foam cell number density and vertical extent of the foam structure. It may be possible that for larger foam patches, larger amounts of air were entrained per unit sea surface area than for smaller foam patches. Larger void fractions of air could produce a denser foam structure which takes longer to decay simply due to an increase in the density of foam cells.

[61] The temporal variation in whitecap foam decay times is illustrated by the observed differences in decay times between periods I and II and periods III and IV (see Figure 8). First, decay times were a factor of 3–4 lower in period III compared to period I and II. Laboratory work by Bock and Frew [1993] has shown that SSM properties, such as surface elasticity, can increase with time after SSM formation in the laboratory. The change in elasticity that they measured implied a compositional change in the SSM which demonstrated a progressive selection toward more hydrophobic, insoluble surfactants within the SSM. It is possible therefore, that the SSM composition is impacted by the history of surface convergent motions and wind-forcing preceding an observational period. For the 24 h period immediately prior to observation period III the average wind speed was 2.7 m/s. The onset of visible whitecapping has been reported to occur at a wind speed around 3.0–3.7 m/s [Monahan and O’Muircheartaigh, 1986; Callaghan *et al.*, 2008b] implying that SSM disruption via white capping was unlikely during the 24 h time period prior to period III. We confirmed this by visual inspection of images taken on YD 301 in which the sea surface was calm and had a smooth, glassy appearance. Similar to the laboratory observations of Bock and Frew [1993], it is possible that during this calm period, aging of the SSM through competitive adsorption could have led to changes in the SSM composition resulting in a high ratio of insoluble to soluble surfactants. The destabilizing effect of high film pressures associated with the build-up of insoluble surfactants, as found by G67, during the preceding calm period could therefore explain the low decay times observed in period III. Equally plausible is that wave breaking was simply less vigorous during period III than periods I and II due to the low wind speed. Leifer *et al.* [2006] noted that more intense plunging breakers produced both diffuse and dense bubble plumes whereas spilling breakers tended to produce diffuse plumes only. If spilling breakers were more common during the low wind speeds of period III, then it may be expected that they produced more diffuse bubble plumes resulting in faster decaying whitecaps. For this to be relevant to the present study, the surface whitecap area above dense and diffuse plumes would have to be similar since we found no significant statistical difference in the generation of maximum foam patch area between all 4 periods (see Figure 10). Additionally, Leifer and de Leeuw [2006] showed that diffuse bubble plumes generally have shallower penetration depths than dense bubble plumes. This could therefore act to limit the amount of surfactant coating due to decreased time below the water surface.

[62] The rapid increase in wind speed between period III and period IV coincided with an increase in whitecap decay times in period IV relative to period III, but still less than periods I and II, along with increased scatter in decay times. The increased scatter may indicate a transition period during

which there was a change in the composition of the SSM in response to increasing breaking rates and bubble scavenging, or an increase in bubble plume density from more vigorous wave breaking. An important result hypothesized by G67 is that increases in the relative concentration of insoluble to soluble surfactants in the SSM leads to a decrease in bubble lifetimes and bubble lifetimes should be expected to be longer when both the inner and outer bubble surface is coated by soluble surfactants only. G67 noted that a minimum period of between 30s and 1 min was needed for insoluble SSM reformation between bubble events to make repeatable measurements of bubble lifetimes. Increased breaking rates from period III to period IV could have limited the time for SSM reformation (from insoluble surfactants) between breaking wave events and may also have generated a greater net upward transport of soluble surfactants into the SSM which would increase the ratio of soluble to insoluble surfactants and thus tend to stabilize the foam. The increased scatter in foam decay times may be indicative of spatial patchiness of SSM composition as a result of a transition in SSM composition due to net upward bubble transport of surfactant and decreased insoluble SSM reformation time. Indeed, SSM properties have been found to vary on scales of meters in previous studies [e.g., *Bock and Frew*, 1993].

[63] The increase in wind speed between period III and period IV may have led to changes in wave breaking properties and therefore bubble plume properties. A change in the proportion of plunging to spilling breakers could have led to increases in the bubble density within bubble plumes. Indeed, *Romero et al.* [2012] have shown a positive correlation between wave slope and the strength of, or amount of energy dissipated by, a breaking wave. We compared the four values of the effective foam decay time (see Table 5) with the average wave slope (see Table 1) for each observational period but we did not find any systematic relationship. However, a dedicated study considering the effect of wave slope on foam decay times on a wave by wave basis is needed to determine if a transition from small breaking slope to large breaking slope (spilling to plunging breakers) affects the lifetime of the associated whitecap foam. As stated above, our measurement of foam decay is based on choosing an appropriate optical threshold to discriminate between whitecap foam and unbroken background water. It does not provide any information about foam depth or foam cell density. Presently it is not fully understood if, for a given set of bubble plume dimensions, the surface whitecap has the same appearance whether formed by a diffuse or dense bubble plume. However, as stated above, it may be reasonable to assume that a denser foam patch could decay more slowly than a more diffuse one with a lower cell concentration.

[64] Finally, the observed temporal variation in foam decay times between periods may have been due to surfactant variability resulting from the passage of different water masses with different bulk properties. Tidal currents in the region regularly reach speeds of 0.5 m s^{-1} which may lead to advection of distinct water masses over several kilometers during a single tidal period, although if this is the case it was not reflected in significant changes in either water temperature or salinity for this study.

[65] We do not have the necessary in situ surfactant measurements or relevant measurements of bubble plumes or breaking wave slopes to categorically state whether or not

changes in these parameters influenced the whitecap foam decay times. However, our review of the foam physics literature, the laboratory experiments on single bubble stability and the changes in bubble plume characteristics with wave breaking type, we believe, all provide plausible explanations for the observed differential whitecap foam decay times.

5. Conclusions

[66] In the published whitecap coverage literature, there have been comparatively few records devoted to measuring the decay time of whitecap foam from individual breaking waves. Field measurements of the total whitecap coverage have largely encompassed the contribution from both actively breaking waves and decaying whitecap foam patches. However, both stages of whitecap coverage represent very different physical processes. Stage A whitecaps, formed by actively breaking waves, are surface expressions of bubble entrainment rates, ambient noise generation, wave energy dissipation, aerosol generation and bubble mediated air-sea gas exchange. Stage B whitecaps represent the decaying of whitecap foam which is important for aerosol generation, and as discussed earlier, decay times are potentially influenced by both bubble plume lifetimes and surfactants. The ratios of Stage B to Stage A whitecap coverage has been estimated at between 1.5 and 40. While some of this variation may include effects from different observation platforms and analysis techniques, Stage B whitecap foam can be expected to dominate estimates of the total whitecap coverage. Knowledge of the extent and variation of Stage B whitecap coverage is important if scatter within single data sets of whitecap coverage and variations between different data sets are to be fully understood.

[67] We have presented the decay time of the surface area of whitecap foam for 552 breaking waves at a single location over a 10-day period. In agreement with other studies, the mean whitecap foam decay, as determined by our optical threshold technique, was adequately described by a simple exponential decay model. The values of the exponential decay constant, τ , varied by about up to a factor of 50 across all individual breaking wave events between 0.2 s to 10.4 s. A significant positive correlation was found between τ and the maximum foam patch area, A_o , for all 4 observation periods. Additionally there was a significant difference in decay times for foam patches of the same size between different observation periods. In general, larger decay times coincided with higher wind speeds. A very weak correlation was found between the decay time of whitecap foam and the average speed of the breaking wave. The maximum foam patch area of each whitecap had a strong positive correlation with the product of the average breaking wave crest length and the breaking distance (the active breaking area).

[68] We did not make all the appropriate in situ measurements to fully understand why whitecap foam decay exhibited scale and time dependent variations. However, we can reasonably assume that the systematic variation was not caused by variations in salinity or water temperature. From a review of the foam physics literature, relevant laboratory-based experiments on single bubble stability in the presence of surfactants and previous laboratory-based observations of a wide variety of wave breaking dependent bubble plume characteristics, we have proposed that the variations in foam

decay times reflect complex bubble-surfactant interactions, surfactant transport, composition, concentration and solubility and varying bubble plume characteristics. We propose that both bubble plume dynamics and surfactants play a role in whitecap foam decay time. The lower limit of foam lifetime is presumably determined by the lifetime of bubble plumes, as already suggested by *Monahan and O'Muircheartaigh* [1986]. Since soluble surfactants (and insoluble surfactants in suitably low concentrations) stabilize foam films, this lower limit may be extended by the presence of surface active materials scavenged by bubbles rising into the foam.

[69] In addition to helping explain differences reported in measured values of W between different data sets, the implications of variations in τ for understanding the physics controlling whitecap foam decay could be far-reaching. Accurate parameterizations of primary marine aerosol flux using the whitecap method require knowledge of an effective whitecap foam decay time. This effective decay time varied by up to a factor of 3.4 for our study and was systematically different to the canonical value of 3.53 s that is often used [*Monahan et al.*, 1982; *Lewis and Schwartz*, 2004]. Also, it has been assumed that measurements of total whitecap coverage are proportional to energy dissipation from breaking waves but our data suggest that without knowledge of decay times of whitecap foam, this assumption may be prone to unknown and systematic errors. It may be more accurate to assume that wave energy dissipation is proportional to Stage A whitecap coverage and not total whitecap coverage. The depth of foam on the sea surface has been shown experimentally and theoretically to be major factors in controlling its microwave emissivity [see *Reul and Chapron*, 2003, and references therein]. This in turn affects satellite based retrievals of sea surface brightness temperature, a critical measurement for the accurate retrieval of satellite based estimates of sea surface salinity and for making direct estimates of W itself.

[70] In light of the implications posed by variable whitecap foam decay time, further laboratory and field experiments are needed to confirm the findings of this study and to investigate the proposed connection between whitecap foam decay times and surfactant concentration and bubble plume characteristics. The outcomes of these studies would potentially lead to more accurate regional and temporal parameterizations of whitecap coverage. Photographic measurements of the sea surface wave spectrum have been used in the past to provide information on the presence of surface slicks of surfactants [*Cini et al.*, 1983]. Similarly, exploring the link between surfactant concentration and rates of decay of whitecap foam, could lead to the development of an optical remote sensing technique capable of determining surfactant presence, absence and concentration. Additionally, if future studies find a direct link between whitecap foam decay time and bubble plume characteristics, air-entrainment rates and volumes may be able to be determined from oceanic observations of whitecap decay times using above water digital images.

[71] **Acknowledgments.** We gratefully acknowledge financial support from the National Science Foundation, Physical Oceanography Division (grant 1061050) and The Office Of Naval Research, Ocean Acoustics Division (grants N00014-10738 and N00014-11030). We would also like to thank James Preisig for his considerable efforts in organizing and running the SPACE08 experiment. Additional financial support for AHC was provided by the Irish Research Council, co-funded by Marie Curie Actions under FP7. We acknowledge the support of James Uyloan in experimental preparation and setup.

References

- Angelova, M. D., and F. Webster (2006), Whitecap coverage from satellite measurements: A first step towards modeling the variability of oceanic whitecaps, *J. Geophys. Res.*, *111*, C03017, doi:10.1029/2005JC003158.
- Banner, M. L., and W. L. Peirson (2007), Wave breaking onset and strength for two-dimensional deep-water wave groups, *J. Fluid Mech.*, *585*, 93–115, doi:10.1017/S0022112007006568.
- Barger, W. R., W. H. Daniel, and W. D. Garrett (1974), Surface chemical properties of banded sea slicks, *Deep Sea Res. Oceanogr. Abstr.*, *21*, 83–89.
- Bock, E. J., and N. M. Frew (1993), Static and dynamic response of natural multicomponent oceanic surface films to compression and dilation: Laboratory and field observations, *J. Geophys. Res.*, *98*, 14,599–14,617, doi:10.1029/93JC00428.
- Bondur, V. G., and E. A. Sharkov (1982), Statistical properties of whitecaps on a rough sea, *Oceanology, Engl. Transl.*, *22*, 274–279.
- Callaghan, A. H., and M. White (2009), Automated processing of sea surface images for the determination of whitecap coverage, *J. Atmos. Oceanic Technol.*, *26*, 383–394, doi:10.1175/2008JTECH0634.1.
- Callaghan, A. H., G. Deane, and M. D. Stokes (2008a), Observed physical and environmental causes of scatter in whitecap coverage values in a fetch limited coastal zone, *J. Geophys. Res.*, *113*, C05022, doi:10.1029/2007JC004453.
- Callaghan, A. H., G. de Leeuw, L. H. Cohen, and C. D. O'Dowd (2008b), The relationship of oceanic whitecap coverage to wind speed and wind history, *Geophys. Res. Lett.*, *35*, L23609, doi:10.1029/2008GL036165.
- Camps, A., et al. (2008), Determination of the sea surface emissivity at L-band and application to SMOS salinity retrieval algorithms: Review of the contributions of the UPC-ICM, *Radio Sci.*, *43*, RS3008, doi:10.1029/2007RS003728.
- Cini, R., P. P. Lombardini, and H. Hühnerfuss (1983), Remote sensing of marine slicks utilizing their influence on wave spectra, *Int. J. Remote Sens.*, *4*(1), 101–110, doi:10.1080/01431168308948533.
- Deane, G. B., and M. D. Stokes (2002), Scale dependence of bubble creation mechanisms in breaking waves, *Nature*, *418*, 839–844, doi:10.1038/nature00967.
- de Leeuw, G., E. L. Andreas, M. D. Angelova, C. W. Fairall, E. R. Lewis, C. O'Dowd, M. Schulz, and S. E. Schwartz (2011), Production flux of sea spray aerosol, *Rev. Geophys.*, *49*, RG2001, doi:10.1029/2010RG000349.
- Dulov, V. A., V. N. Kudryavstev, and A. N. Bol'shakov (2002), A field study of whitecap coverage and its modulations by energy containing surface waves, in *Gas Transfer at Water Surfaces, Geophys. Monogr. Ser.*, vol. 127, edited by M. A. Donelan et al., pp. 187–192, AGU, Washington, D. C., doi:10.1029/GM127p0187.
- Duncan, J. H. (1981), An experimental investigation of breaking waves produced by a towed hydrofoil, *Proc. R. Soc. London, Ser. A.*, *377*, 331–348.
- Ermakov, S. A., S. G. Salashim, and A. R. Panchenko (1992), Film slicks on the sea surface and some mechanisms of their formation, *Dyn. Atmos. Oceans*, *16*, 279–304, doi:10.1016/0377-0265(92)90010-Q.
- Frouin, R., M. Schwindling, and P.-Y. Deschamps (1996), Spectral reflectance of sea foam in the visible and near-infrared: In situ measurements and remote sensing implications, *J. Geophys. Res.*, *101*, 14,361–14,371, doi:10.1029/96JC00629.
- Garrett, W. D. (1967a), Stabilization of air bubble at the air-sea interface by surface active material, *Deep Sea Res. Oceanogr. Abstr.*, *14*, 661–672.
- Garrett, W. D. (1967b), The organic chemical composition of the ocean surface, *Deep Sea Res. Oceanogr. Abstr.*, *14*, 221–227.
- Gemmrich, J. R., and D. M. Farmer (1999), Observations of the scale and occurrence of breaking surface waves, *J. Phys. Oceanogr.*, *29*, 2595–2606, doi:10.1175/1520-0485(1999)029<2595:OOTSAO>2.0.CO;2.
- Gemmrich, J. R., M. L. Banner, and C. Garrett (2008), Spectrally resolved energy dissipation rate and momentum flux of breaking waves, *J. Phys. Oceanogr.*, *38*, 1296–1312, doi:10.1175/2007JPO3762.1.
- Goddijn-Murphy, L., D. K. Woolf, and A. H. Callaghan (2011), Parameterizations and algorithms for oceanic whitecap coverage, *J. Phys. Oceanogr.*, *41*, 742–756, doi:10.1175/2010JPO4533.1.
- Gordon, H. R. (1997), Atmospheric correction of ocean color imagery in the Earth Observing System Era, *J. Geophys. Res.*, *102*(D14), 17,081–17,106, doi:10.1029/96JD02443.
- Henry, C. L. (2010), Bubbles, thin films and ion specificity, PhD thesis, 220pp., Aust. Natl. Univ., Canberra.
- Holthuijsen, L. H. (2007), *Waves in Oceanic and Coastal Waters*, Cambridge Univ. Press, Cambridge, U. K.
- Holthuijsen, L. H., and T. H. C. Herbers (1986), Statistics of breaking waves observed as whitecaps in the open sea, *J. Phys. Oceanogr.*, *16*, 290–297, doi:10.1175/1520-0485(1986)016<0290:SOBWOA>2.0.CO;2.
- Hwang, P. A., and M. A. Sletten (2008), Energy dissipation of wind-generated waves and whitecap coverage, *J. Geophys. Res.*, *113*, C02012, doi:10.1029/2007JC004277.

- Jähne, B., W. Huber, A. Dutzi, T. Wais, and J. Ilmberger (1984), Wind/wave tunnel experiments on the Schmidt number and wave field dependence of air-water gas exchange, in *Gas Transfer at Water Surfaces*, *Geophys. Monogr. Ser.*, vol. 127, edited by M. A. Donelan et al., pp. 303–309, AGU, Washington, D. C., doi:10.1029/GM127p0187.
- Kleiss, J. M., and W. K. Melville (2010), Observations of wave-breaking kinematics in fetch-limited seas, *J. Phys. Oceanogr.*, *40*, 2575–2604, doi:10.1175/2010JPO4383.1.
- Kleiss, J. M., and W. K. Melville (2011), The analysis of sea surface imagery for whitecap kinematics, *J. Atmos. Oceanic Technol.*, *28*, 219–243, doi:10.1175/2010JTECH0744.1.
- Kujawinski, E. B., J. W. Farrington, and J. W. Moffett (2002), Evidence for grazing-mediated production of dissolved surface-active material by marine protists, *Mar. Chem.*, *77*, 133–142, doi:10.1016/S0304-4203(01)00082-2.
- Lafon, C., J. Piazzola, P. Forget, O. Le Calve, and S. Despiau (2004), Analysis of the variations of the whitecap fraction as measured in a coastal zone, *Boundary Layer Meteorol.*, *111*, 339–360, doi:10.1023/B:BOUN.0000016490.83880.63.
- Lafon, C., J. Piazzola, P. Forget, and S. Despiau (2007), Whitecap coverage in coastal environment for steady and unsteady wave field conditions, *J. Mar. Syst.*, *66*, 38–46, doi:10.1016/j.jmarsys.2006.02.013.
- Leifer, I., and G. de Leeuw (2006), Bubbles generated from wind-steepened breaking waves: 1. Bubble plume bubbles, *J. Geophys. Res.*, *111*, C06020, doi:10.1029/2004JC002673.
- Leifer, I., G. Caulliez, and G. de Leeuw (2006), Bubbles generated from wind-steepened breaking waves: 2. Bubble plumes, bubbles and wave characteristics, *J. Geophys. Res.*, *111*, C06021, doi:10.1029/2004JC002676.
- Lewis, E. R., and S. E. Schwartz (Eds.) (2004), *Sea Salt Aerosol Production: Mechanisms, Methods, Measurements and Models—A Critical Review*, *Geophys. Monogr. Ser.*, vol. 152, 413pp., AGU, Washington, D. C.
- Lippmann, T. C., and R. A. Holman (1989), Quantification of sand bar morphology: A video technique based on wave dissipation, *J. Geophys. Res.*, *94*, 995–1011, doi:10.1029/JC094iC01p00995.
- Liss, P. S. (1975), Chemistry of the sea-surface microlayer, in *Chemical Oceanography*, vol. 2, edited by J. P. Riley and G. Skirrow, pp. 193–244, Academic, London.
- Liss, P. S., and R. A. Duce (Eds.) (1997), *The Sea Surface and Global Change*, 519pp., Cambridge Univ. Press, Cambridge, U. K., doi:10.1017/CBO9780511525025.
- Manev, E. D., and A. V. Nguyen (2005), Critical thickness of microscopic thin liquid films, *Adv. Colloid Interface Sci.*, *114–115*, 133–146, doi:10.1016/j.cis.2004.07.013.
- Melville, W. K., and P. Matusov (2002), Distribution of breaking waves at the ocean surface, *Nature*, *417*, 58–63, doi:10.1038/417058a.
- Mironov, A. S., and V. A. Dulov (2008), Detection of wave breaking using sea surface video records, *Meas. Sci. Technol.*, *19*, 015405, doi:10.1088/0957-0233/19/1/015405.
- Monahan, E. C. (1971), Oceanic Whitecaps, *J. Phys. Oceanogr.*, *1*, 139–144, doi:10.1175/1520-0485(1971)001<0139:OW>2.0.CO;2.
- Monahan, E. C., and M. Lu (1990), Acoustically relevant bubble assemblages and their dependence on meteorological parameters, *IEEE J. Oceanic Eng.*, *15*(4), 340–349, doi:10.1109/48.103530.
- Monahan, E. C., and I. O’Muircheartaigh (1986), Whitecaps and the passive remote sensing of the ocean surface, *Int. J. Remote Sens.*, *7*(5), 627–642, doi:10.1080/01431168608954716.
- Monahan, E. C., and C. R. Zietlow (1969), Laboratory Comparisons of fresh-water and salt-water whitecaps, *J. Geophys. Res.*, *74*(28), 6961–6966, doi:10.1029/JC074i028p06961.
- Monahan, E. C., K. L. Davidson, and D. E. Spiel (1982), Whitecap aerosol productivity deduced from simulation tank measurements, *J. Geophys. Res.*, *87*(C11), 8898–8904, doi:10.1029/JC087iC11p08898.
- Monahan, E. C., D. E. Spiel, and K. L. Davidson (1986), A model of marine aerosol generation via whitecaps and wave disruption, in *Oceanic Whitecaps and Their Role in Air-Sea Exchange Processes*, edited by E. C. Monahan and G. MacNiochail, pp. 167–174, Springer, New York, doi:10.1007/978-94-009-4668-2_16.
- Nolan, P. F. (1988), Decay characteristics of individual whitecaps, in *Oceanic Whitecaps and the Fluxes of Droplets From, Bubbles to, and Gases Through, the Sea Surface*, *Whitecap Rep. 4*, edited by E. C. Monahan et al., pp. 41–56, Mar. Sci. Inst., Univ. of Conn., Groton.
- Peltzer, R. D., and O. M. Griffin (1988), Stability of a three-dimensional foam layer in seawater, *J. Geophys. Res.*, *93*, 10,804–10,812, doi:10.1029/JC093iC09p10804.
- Phillips, O. M. (1985), Spectral and statistical properties of the equilibrium range in wind-generated gravity waves, *J. Fluid Mech.*, *156*, 505–531, doi:10.1017/S0022112085002221.
- Phillips, O. M., F. L. Posner, and J. P. Hansen (2001), High range resolution radar measurements of the speed distribution of breaking events in wind-generated ocean waves: Surface impulse and wave energy dissipation rates, *J. Phys. Oceanogr.*, *31*, 450–460, doi:10.1175/1520-0485(2001)031<0450:HRRRMO>2.0.CO;2.
- Pounder, C. (1986), Sodium chloride and water temperature effects on bubbles, in *Oceanic Whitecaps and Their Role in Air-Sea Exchange Processes*, edited by E. C. Monahan and G. MacNiochail, p. 278, Springer, New York.
- Prud’homme, R. K., and S. A. Khan (Eds.) (1995), *Foams: Theory, Measurements and Applications*, *Surfactant Sci. Ser.*, vol. 57, Marcel Dekker, New York.
- Pugh, R. J. (1996), Foaming, foam films, antifoaming and defoaming, *Adv. Colloid Interface Sci.*, *64*, 67–142, doi:10.1016/0001-8686(95)00280-4.
- Quilfen, Y., C. Prigent, B. Chapron, A. A. Mouche, and N. Houti (2007), The potential of QuikSCAT and WindSat observations for the estimation of sea surface wind vector under severe weather conditions, *J. Geophys. Res.*, *112*, C09023, doi:10.1029/2007JC004163.
- Rapp, R. J., and W. K. Melville (1990), Laboratory measurements of deep-water breaking waves, *Philos. Trans. R. Soc. London, Ser. A*, *331*, 735–800, doi:10.1098/rsta.1990.0098.
- Reul, N., and B. Chapron (2003), A model of sea-foam thickness distribution for passive microwave remote sensing applications, *J. Geophys. Res.*, *108*(C10), 3321, doi:10.1029/2003JC001887.
- Romero, L., W. Melville, and J. Kleiss (2012), Spectral energy dissipation due to surface-wave breaking, *J. Phys. Oceanogr.*, doi:10.1175/JPO-D-11-072.1, in press.
- Ross, D. B., and V. Cardone (1974), Observations of oceanic whitecaps and their relation to remote measurements of surface wind speed, *J. Geophys. Res.*, *79*, 444–452, doi:10.1029/JC079i003p00444.
- Salter, M. E., R. C. Upstill-Goddard, P. D. Nightingale, S. D. Archer, B. Blomquist, D. T. Ho, B. Huebert, P. Schlosser, and M. Yang (2011), Impact of an artificial surfactant release on air-sea gas fluxes during Deep Ocean Gas Exchange Experiment II, *J. Geophys. Res.*, *116*, C11016, doi:10.1029/2011JC007023.
- Sharkov, E. A. (2007), *Breaking Ocean Waves: Geometry, Structure and Remote Sensing*, Springer, Chichester, U. K.
- Sheludko, A. (1967), Thin liquid films, *Adv. Colloid Interface Sci.*, *1*, 391–464, doi:10.1016/0001-8686(67)85001-2.
- Sugihara, Y., H. Tsumori, T. Ohga, H. Yoshioka, and S. Serizawa (2007), Variation of whitecap coverage with wave-field conditions, *J. Mar. Syst.*, *66*, 47–60, doi:10.1016/j.jmarsys.2006.01.014.
- Ternes, R. L., and J. C. Berg (1984), The effect of monolayer collapse on bubble stability, *J. Colloid Interface Sci.*, *98*, 471–477.
- Thomson, J., and A. T. Jessup (2009), A Fourier-based method for the distribution of breaking crests from video observations, *J. Atmos. Oceanic Technol.*, *26*, 1663–1671, doi:10.1175/2009JTECH0622.1.
- Thomson, J., J. R. Gemmrich, and A. T. Jessup (2009), Energy dissipation and spectral distribution of whitecaps, *Geophys. Res. Lett.*, *36*, L11601, doi:10.1029/2009GL038201.
- Toba, Y., and M. Chien (1973), Quantitative expression of the breaking of wind waves on the sea surface, *Rec. Oceanogr. Works Jpn.*, *12*, 1–11.
- Weaire, D., and S. Hutzler (Eds.) (1999), *The Physics of Foams*, Clarendon, Oxford, U. K.
- Williams, P., A. Carlucci, S. Henrichs, E. V. Vleet, S. Horrigan, F. Reid, and K. Robertson (1986), Chemical and microbiological studies of sea-surface films in the southern Gulf of California and off the west coast of Baja California, *Mar. Chem.*, *19*, 17–98, doi:10.1016/0304-4203(86)90033-2.
- Woolf, D. K. (1997), Bubbles and their role in gas exchange, in *The Sea Surface and Global Change*, edited by P. S. Liss and R. A. Duce, pp. 173–206, Cambridge Univ. Press, Cambridge, U. K., doi:10.1017/CBO9780511525025.007.
- Wu, J. (1988), Variations of whitecap coverage with wind stress and water temperature, *J. Phys. Oceanogr.*, *18*, 1448–1453, doi:10.1175/1520-0485(1988)018<1448:VOWCWW>2.0.CO;2.
- Wurl, O., L. Miller, R. Röttgers, and S. Vagle (2009), The distribution and fate of surface-active substances in the sea-surface microlayer and water column, *Mar. Chem.*, *115*, 1–9, doi:10.1016/j.marchem.2009.04.007.
- Wurl, O., E. Wurl, L. Miller, K. Johnson, and S. Vagle (2011), Formation and distribution of sea-surface microlayers, *Biogeosciences*, *8*, 121–135, doi:10.5194/bg-8-121-2011.
- Zhao, D., and Y. Toba (2001), Dependence of whitecap coverage on wind and wind-wave properties, *J. Oceanogr.*, *57*, 603–616, doi:10.1023/A:1021215904955.
- Žutić, V., B. Čosović, E. Marčenko, N. Bihari, and F. Kršinić (1981), Surfactant production by marine phytoplankton, *Mar. Chem.*, *10*, 505–520.